This is a preprint submitted to EarthArXiv. This manuscript has been peer-reviewed and is in revision in Contributions to Minerology and Petrology.

Phase-equilibrium geobarometers for silicic rocks based on rhyolite-MELTS. Part 5: Principles for multiple-phase geobarometry with examples from plagioclase + orthopyroxene ± quartz ± magnetite assemblages

Sarah L. Smithies

Corresponding author

School of Earth and Environment, University of Canterbury, Christchurch, New Zealand

https://orcid.org/0000-0002-7734-2952

sarah.smithies@canterbury.ac.nz

Guilherme A. R. Gualda

Department of Earth and Environmental Sciences, Vanderbilt University, TN, USA

https://orcid.org/0000-0003-0720-2679

Lydia J. Harmon

Department of Geology, Occidental College, CA, USA

https://orcid.org/0000-0002-9985-705X

Keywords:

This is a preprint submitted to EarthArXiv. This manuscript has been peer-reviewed and is in revision in Contributions to Minerology and Petrology.

Geobarometry, rhyolite-MELTS, phase equilibrium, thermodynamics, Taupō Volcanic Zone, Puyehue-Cordón Caulle

This is a preprint submitted to EarthArXiv. This manuscript has been peer-reviewed and is in revision in Contributions to Minerology and Petrology.

Abstract

The quartz + feldspar rhyolite-MELTS phase-equilibrium geobarometer is a useful tool for calculating equilibration pressures of rhyolitic magmas. However, it is somewhat limited by typically requiring quartz saturation in magma. Here, we employ the principles from Parts 1-4 to move beyond modeling a specific mineral assemblage. We demonstrate methods for carefully interpreting rhyolite-MELTS geobarometry results to constrain multiple-phase equilibration pressure in quartz-undersaturated dacites to rhyolites, and where quartz saturation is uncertain. We show examples of storage pressure calculations from quartz-absent rhyodacites to rhyolites from Puyehue-Cordón Caulle (PCC), Chile and examples of equilibration between extracted rhyolitic melt compositions and unknown mush mineral assemblages from the Taupō Volcanic Zone, New Zealand. In these cases, orthopyroxene + plagioclase pressures can be used. However, orthopyroxene saturation pressure results are higher at lower modelled oxygen fugacity (f_{O2}). This can be resolved by modelling at independently constrained f_{O2}, or by modelling at a range of f_{O2} to search for orthopyroxene + magnetite + feldspar co-saturation. We show that orthopyroxene + magnetite + feldspar pressures for PCC are consistent with results from other geobarometers and occur at f_{O2} values within error of the f_{O2} calculated from Fe-Ti oxides. If quartz saturation is uncertain, quartz + feldspar pressures are a maximum and pyroxene-bearing pressures at low f_{O2} are a minimum. For uncertain mineral assemblages, the coincidence of multiple phases (≥3) saturating together at reasonable f_{O2} could be used to infer the equilibrium mineral assemblage. Careful inspection of rhyolite-MELTS geobarometry results therefore gives nuanced information about equilibration pressure, mineral assemblage, and f_{O2}.

Introduction

A fundamental problem in igneous petrology is constraining the pressure of magmatic processes during evolution, ascent, and eruption. Pressure has critical implications for understanding the processes that drive eruption (Caricchi, et al. 2021; Gonnermann and Manga 2007). Pressures can be converted to depth assuming lithostatic conditions to estimate the depth and geometry of magma bodies (Black and Andrews 2020; Cooper, et al. 2012), and therefore the pre-eruptive architecture of magma systems (Edmonds, et al. 2019; Gualda, et

al. 2018; Wieser, et al. 2023a). These magma system models are useful in combination with geophysical datasets to interpret the unrest signals of modern volcanos (Giordano and Caricchi 2022; Magee, et al. 2018; Pritchard, et al. 2018).

There are many geobarometers that can be used to estimate magmatic pressures from compositional parameters such as mineral compositions (e.g., Hammarstrom and Zen 1986; Jorgenson, et al. 2022; Mutch, et al. 2016; Putirka 2008; Ridolfi, et al. 2010), volatile contents in melt inclusions (e.g., Anderson Jr, et al. 1989; Burnham 1994; Liu, et al. 2005; Newman and Lowenstern 2002; Papale, et al. 2006; Wallace, et al. 1995), and melt major-element compositions (e.g., Blundy 2022; Blundy and Cashman 2001; Gualda and Ghiorso 2013b; Gualda and Ghiorso 2014; Herzberg 2004; Voigt, et al. 2017; Weber and Blundy 2024; Wilke, et al. 2017; Yang, et al. 1996). Melt geobarometers (geobarometers that use just the melt composition as the input, see Ubide, et al. (in press)), search for the pressure that melt of a known composition equilibrated with mineral phases of interest. A distinct advantage of melt geobarometers is that major-element melt compositions are relatively easy to obtain (by X-ray fluorescence spectroscopy – XRF, wavelength dispersive X-ray spectroscopy using an electron microprobe – WDS-EMP, or energy dispersive X-ray spectroscopy using a scanning electron microprobe – EDS-SEM) compared to other common geobarometry techniques (e.g., measuring H_2O-CO_2 in melt inclusions by Fourier transform infrared spectroscopy or secondary ion mass spectrometry; measuring mineral rim and core compositions by WDS-EMP). Unlike geobarometers that use the composition of multiple phases (e.g., amphibole-plagioclase Holland and Blundy 1994; Molina, et al. 2021; orthopyroxene-clinopyroxene, Putirka 2008), melt geobarometers do not require the assumption of equilibrium between paired phase compositions. Melt geobarometers can either be derived from empirical relationships extrapolated from experimental datasets (Blundy 2022; Blundy and Cashman 2001; Herzberg 2004; Voigt, et al. 2017; Weber and Blundy 2024; Wilke, et al. 2017; Yang, et al. 1996), or from phase-equilibria models (Bégué, et al. 2014b; Gualda and Ghiorso 2014; Harmon, et al. 2018; Pamukçu, et al. 2015). We focus on phase-equilibrium geobarometers, which have the advantage of being grounded in thermodynamic theory and better suited to interpolation and extrapolation to unknown compositions.

Melt geobarometers, in combination with mineral geobarometers, are useful for determining the pressure evolution of a magma system as magma travels and is stored through the crust. In pyroclastic rocks with rapidly quenched glass, we can assume that the matrix glass represents the melt in pre-eruptive storage. Here, we define "pre-eruptive storage pressure" as the pressure that the melt with the matrix glass composition equilibrated with the autocrystic mineral assemblage (see Ubide, et al. in press), which we can infer from the observed mineral assemblage (Figure 1). Additionally, we can assume that the bulk composition of erupted magma represents the composition of the melt that equilibrated with the mush (Figure 1; Blundy 2022; Gualda, et al. 2019b). We define the pressure that a melt composition equilibrated with the inferred mush mineral assemblage – which we can infer from whole-rock compositions – as "extraction pressure" (Gualda, et al. 2019b). Melt geobarometers can therefore give pressures for at least two stages of magma evolution prior to eruption (Gualda, et al. 2024; Gualda, et al. 2019b; Seropian, et al. 2021; Smithies, et al. 2023).

In the last decade, there have been rapid advancements in using phase-equilibria to find the pre-eruptive storage pressures and extraction pressures of rhyolitic magmas (Bégué, et al. 2014b; Gualda and Ghiorso 2014; Gualda, et al. 2019b; Harmon, et al. 2018; Pamukçu, et al. 2015). Gualda and Ghiorso (2014) introduced a geobarometer that searches for the equilibration pressure between melt, quartz, and one or two feldspars (hereafter referred to as the "quartz + feldspar geobarometer"). The Gualda and Ghiorso (2014) quartz + feldspar geobarometer uses the rhyolite-MELTS version 1.0 model to calculate the equilibration pressure of quartz, feldspars, and melt. The quartz + feldspar geobarometer has been applied to many silicic systems, including the Taupō Volcanic Zone (Bégué, et al. 2014b; Gualda, et al. 2018; Gualda, et al. 2019b; Harmon, et al. 2024a; Harmon, et al. 2024b; Pamukçu, et al. 2021; Pamukçu, et al. 2020; Smithies, et al. 2024; Smithies, et al. 2023), Peach Spring Tuff, Silver Creek Caldera (Foley, et al. 2020; Pamukçu, et al. 2015), Bishop Tuff, Long Valley Caldera (Gualda and Ghiorso 2013a; Gualda, et al. 2022), the Youngest Toba Tuff, northern Sumatra (Pearce, et al. 2020); and Hokkaido, Japan (Pitcher, et al. 2021), among others. Generally, rhyolite-MELTS quartz + feldspar geobarometry results compare well to independent volatile and amphibole geobarometry estimates on the same systems (Bégué, et al. 2014b; Gualda, et al. 2019a; Pamukçu, et al. 2015; Pamukçu, et al. 2021). The precision of the quartz + feldspar

geobarometry results calculated from XRF and EDS-SEM compositions is on the order of 10-20 MPa 1σ (Gualda, et al. 2024; Pamukçu, et al. 2021; Pitcher, et al. 2021; Smithies, et al. 2024; Smithies, et al. 2023). These errors are equivalent to 0.4-0.8 km depth, assuming a crustal density of 2.7 g cm^{-3}, making the quartz + feldspar geobarometer a useful and relatively precise estimate of pressure and depth.

Although the rhyolite-MELTS quartz + feldspar geobarometer is useful in many rhyolitic systems, it is limited to magma that is saturated in quartz. This limits its usefulness to rhyolitic compositions, and to magma where we know the equilibrium mineral assemblage with confidence. This is a potential problem, as the mineral assemblage in volcanic rocks is often a complex mixture of crystals grown in equilibrium with the surrounding melt/glass ("autocrysts"), and crystals incorporated from other parts of the magmatic system or from the country rock ("antecrysts" and "xenocrysts") (e.g., Bachmann, et al. 2002; Ubide, et al. in press). The rock mineral assemblage is therefore not unequivocal proof of the equilibrium mineral assemblage.

Uncertainty over whether or not quartz is saturated is also a significant limitation of using rhyolite-MELTS geobarometry to calculate extraction pressure (Figure 1). Here, we search for the pressure that a melt with the bulk-rock composition equilibrated with the mush. In this scenario, quartz saturation is uncertain as we must infer the mineral assemblage of the mush from erupted mush fragments or from the composition of the erupted magma. This leaves us with the question: how can phase-equilibria models be used to constrain pressure for systems where we are uncertain if quartz is saturated?

Harmon, et al. (2018) introduced a geobarometer that uses the same rhyolite-MELTS thermodynamic model as Gualda and Ghiorso (2014) but searches for the pressure of equilibration between feldspar (typically plagioclase) and one or two pyroxenes (hereafter the "plagioclase + pyroxene geobarometer"). Harmon, et al. (2018) tested the plagioclase + pyroxene geobarometer on basaltic-andesite compositions and found that it could find reasonable pressure estimates (e.g., 50 – 150 MPa for a Mt. Ruapehu case-study, compared to independent volatile pressures of 50 – 230 MPa for the same volcano (Kilgour, et al. 2013)). Other studies subsequently applied the plagioclase + pyroxene geobarometer to dacitic to rhyolitic systems (Foley, et al. 2020; Gualda, et al. 2019b; Harmon, et al. 2024b; Pamukçu, et

al. 2021; Smithies, et al. 2024; Smithies, et al. 2023). The plagioclase + pyroxene geobarometer is sensitive to oxygen fugacity (f_{O2}) due to the strong partitioning of Fe^{2+} relative to Fe^{3+} in pyroxene. Although independently estimated f_{O2} (e.g. from Fe-Ti oxides) can be used as an input into the geobarometry calculation, there is some uncertainty over whether the f_{O2} estimated from Fe-Ti oxides records pre-eruptive conditions, or whether it may have re-equilibrated during syn-eruptive conditions (Pitcher, et al. 2021; Tomiya, et al. 2013). This makes constraining pressure with the plagioclase + pyroxene geobarometer challenging.

The goal of this study is to demonstrate the efficacy of the rhyolite-MELTS geobarometer across a range of different observed and inferred mineral assemblages. By combining our understanding of plagioclase + pyroxene phase-equilibria geobarometry (Harmon, et al. 2018) with our understanding of quartz + feldspar phase-equilibria geobarometry (Gualda and Ghiorso 2014) to better constrain pressure in quartz-undersaturated dacites and rhyolites, we demonstrate that the principles established in this series (Bégué, et al. 2014b; Gualda and Ghiorso 2014; Harmon, et al. 2018; Pamukçu, et al. 2015) can be adapted to a wider range of igneous systems. We explore examples from two systems: extraction of rhyolitic magma from an unknown mush mineral assemblage in the Taupō Volcanic Zone (TVZ), Aotearoa New Zealand; and pre-eruptive magma storage (i.e., depth of melt equilibration with autocrysts) of quartz-absent rhyodacites to rhyolites from Puyehue-Cordón Caulle (PCC), Chile. Using these case studies, we demonstrate that rhyolite-MELTS geobarometry results can be interpreted to give a more nuanced understanding of melt pressures in the presence or absence of quartz.

Methods

Modelling approach for determining pressure and equilibrium mineral assemblage

In Figure 2 we show an example of a quartz + feldspar geobarometry result following the method of Gualda and Ghiorso (2014). The calculations were performed on a pressure-temperature grid, calculating the equilibrium assemblage at 1°C temperature steps and 25 MPa pressure steps. The melt composition that we were interested in was input as the bulk composition of the system (in the Figure 2 example, a whole-rock composition from a single pumice clast was used to give an extraction pressure). The saturation surfaces represent the

highest temperature that each mineral phase is present for a given pressure. The saturation surfaces were interpolated between each 25 MPa interval.

At high temperatures, the simulated magma is liquid (i.e. above the liquidus) with an exsolved fluid phase. Therefore, above the liquidus, the melt composition is the same as the bulk composition of the system. At temperatures below the liquidus, the system has liquid, solids and an exsolved fluid phase. This means that below the liquidus, crystallization of solid phases changes the composition of the melt, such that the simulated melt does not have the same composition as the bulk composition. This is an important realization, as only the region at or above the liquidus has melt with the same composition as the bulk composition of the system, which is the measured composition input by the user (either a whole-rock or glass composition). Therefore, only pressures and temperatures in the region at or above the liquidus are acceptable for the measured melt composition, while the region below the liquidus does not yield acceptable pressure or temperature solutions for the measured melt composition. If we are searching for an equilibrium assemblage of melt (represented by the measured composition) and minerals, the only part of the diagram in Figure 2 where this is possible is at the liquidus. In the example in Figure 2, if we assume that both orthopyroxene and plagioclase are in equilibrium with the input melt composition, there is only one possible pressure and temperature, at 106 MPa and 800 °C. The intersection of the orthopyroxene and plagioclase saturation surfaces, therefore, gives us the pressure of equilibration between orthopyroxene, plagioclase, and melt of the given composition. The saturation surface intersection also gives a temperature result that could be quantified. However, temperature, unlike pressure, is very sensitive to water activity (Johannes and Holtz 1996). We therefore do not quantify temperatures here.

The saturation surfaces are interpolated between the 25 MPa pressure intervals. To calculate the saturation surface intersections, we use the parabola-fitting procedure described by Gualda and Ghiorso (2014). The residual temperature between the saturation surfaces at each 25 MPa interval is calculated, then a parabola is fitted to the minimum residual and two points on either side of the minimum (Figure 2). This parabola-fitting procedure is only applied if the minimum is ≤ 5 °C (the minimum temperature threshold in Figure 2). Gualda and Ghiorso (2014) show that the minimum of the parabola is a satisfactory estimate of the saturation

surface intersection. When the minimum of the residual curve is never ≤ 5 °C over the pressure range investigated, we conclude that the rhyolite-MELTS geobarometer finds no satisfactory pressure for the melt composition and mineral assemblage of interest.

Case study geobarometry calculations

We show examples from two case studies: rhyolites of the Taupō Volcanic Zone (TVZ), Aotearoa New Zealand; and rhyodacites to rhyolites from Puyehue-Cordón Caulle (PCC), Chile. From the TVZ, we show examples of extraction pressure calculations, using whole-rock compositions to model the pressure at which the eruptible magma was extracted from a mush with unknown mineral assemblage (Figure 1). We focus on eruptions that have low crystal contents (<8% by vol.) to minimize the potential impact of entrained antecrysts and xenocrysts into the results. The TVZ was selected as an example of a system where the erupted magma is quartz-bearing, but the mineralogy of the mush is uncertain (Table 1). From PCC, we show examples of pre-eruptive storage pressure calculations, using glass compositions to model the pressure the melt was in equilibrium with the phenocryst assemblage immediately prior to eruption. In contrast to the TVZ, PCC rhyolites do not have quartz in either the phenocryst mineral assemblage (Table 1) or in the co-erupted mush fragments (Winslow, et al. 2022).

In the TVZ, we focus on five large (>50 km^3 dense rock equivalent), caldera-forming eruptions (Table 1). Previously published whole-rock compositions were collated from Smithies, et al. (2023). Each sample (n=53) is an individual pumice clast collected from unwelded ignimbrite deposits. Whole-rock compositions were collected by either XRF (Chimp, Pokai, Kaingaroa, and Mamaku samples) or by inductively coupled plasma optical emission spectrometry (Ohakuri samples). The pumice clasts have sparse (<8% by vol.) plagioclase + orthopyroxene + Fe-Ti oxides ± quartz ± hornblende ± clinopyroxene phenocrysts (Table 1). All the samples are rhyolitic in composition (Figure 3).

For each TVZ composition, we collated geobarometry calculations from Smithies, et al. (2023) and performed additional calculations with the same methodology to expand the range of f_{O2} values. Geobarometry calculations were performed with the rhyolite-MELTS v.1.0 model with an updated version of the MELTS_Excel interface (Gualda and Ghiorso 2015). The latest version of MELTS_Excel and supporting documentation is distributed for free from

http://melts.ofm-research.org. Whole-rock compositions were input as the melt composition. Equilibration calculations were performed in a pressure-temperature grid from 500 to 25 MPa in 25 MPa steps and from 1100 °C to 700 °C in 1 °C steps. We forced fluid saturation at all pressures by setting H_2O to 15 wt.%; even though these are unrealistic H_2O contents for most crustal magmas, they guarantee that the simulated magmas are saturated in water. Importantly, Gualda and Ghiorso (2014) show that estimated pressures are not very sensitive to H_2O content for systems with high H_2O activity, as is expected for most crustal magmas that feed eruptions to the surface. Further, Ghiorso and Gualda (2015) demonstrate that estimated pressures are insensitive to H_2O activity when an H_2O-CO_2 fluid phase is present, which is likely the case for the vast majority of rhyolitic magmas. We thus rely on the conclusions from Gualda and Ghiorso (2014) and Ghiorso and Gualda (2015) – which are reinforced by the results in Harmon, et al. (2018) – and suggest the method we propose here should be valid for cases in which H_2O activity is high, and particularly so for cases in which the system is fluid saturated. The calculations were repeated from 0.5 log units below the quartz-fayalite-magnetite (QFM) f_{O2} buffer to 2 log units above it in 0.5 log unit steps (QFM -0.5; QFM; QFM +0.5; QFM +1.0; QFM +1.5; QFM +2.0). For a small subset of samples (POK_105A, POK_112A_A, OHK302B4) we expanded the f_{O2} range to include calculations at QFM -1.0, QFM -1.5, and QFM -2.0.

For the PCC system, we include compositions from the three most recent large eruptions (Table 1). These are relatively small (0.25-1.5 km^3) eruptions, which generated both lava flows and pyroclastic deposits (Lara, et al. 2006; Pistolesi, et al. 2015; Singer, et al. 2008). Compositions were collated from Castro, et al. (2013); Schipper, et al. (2019); Seropian, et al. (2021). The samples (n=33) are individual pyroclastic clasts. Each sample composition is a mean of 9-40 spot compositions measured by WDS-EMP on fresh, unaltered glass. Phenocrysts are sparse in the pyroclastic material (<15 vol.%) with an assemblage of plagioclase + orthopyroxene + clinopyroxene + Fe-Ti oxides (Table 1). The bulk rock and glass compositions are rhyodacitic to rhyolitic (Figure 3).

For each PCC composition, we collated geobarometry calculations from Seropian, et al. (2021) and performed additional calculations with the same methodology to expand the range of f_{O2} values. The input parameters are the same as for the TVZ samples, except that glass

compositions were used to result in pre-eruptive storage pressure estimates (Figure 1), and therefore the pressure-temperature grid was reduced to 400 to 25 MPa in 25 MPa steps and from 1100 °C to 700 °C in 1 °C steps. We set H_2O to 10 wt.% to force fluid saturation (see above). The calculations were repeated from 1 log unit below the nickel-nickel oxide (NNO) f_{O2} buffer to 1.5 log units above in 0.25 or 0.5 log unit steps (NNO -1.0; NNO -0.75; NNO -0.5; NNO -0.25; NNO; NNO +0.5; NNO +1.0; NNO +1.5). For three samples (D60_17, A-gr12, B-gr2) we ran additional calculations at NNO -1.5, NNO -2.0, and NNO -2.5. This is approximately equivalent to the f_{O2} range used for the TVZ samples.

Results

Geobarometry results

For the TVZ, at the lowest f_{O2} tested (QFM -0.5), the extraction pressures range from 68-381 MPa with a mean of 214 MPa (Figure 4). The modelled mineral assemblages are a mixture of orthopyroxene + plagioclase (n=40), quartz + plagioclase (n=5), and plagioclase + orthopyroxene + quartz (n=8). At higher f_{O2}, the mean pressure result is higher (e.g., 291 MPa at QFM +0.5) and there are fewer plagioclase + orthopyroxene results (e.g., n=16 at QFM +0.5) and plagioclase + orthopyroxene + quartz results (e.g., n=1 at QFM +0.5) relative to the number of quartz + plagioclase results (e.g., n=36 at QFM +0.5). At the highest f_{O2} tested (QFM +2), the TVZ extraction pressures range from 122-468 MPa with a mean of 327 MPa. At high f_{O2} (QFM +2) the calculated mineral assemblage is exclusively quartz + plagioclase (n=50).

The PCC results are dominated by a plagioclase + orthopyroxene mineral assemblage at all f_{O2} tested (Figure 4). Quartz-bearing mineral assemblages only occur in a minority of samples (n=3) at the highest f_{O2} values we tested (NNO +1 and NNO +1.5). The pressure results are strongly dependent on f_{O2}. At the lowest f_{O2} tested (NNO -1.0) the pressures are relatively low, ranging from 25-123 MPa with a mean of 80 MPa. At progressively higher f_{O2} values, the pressures increase. At the highest f_{O2} tested (NNO +1.5), the pressures range from 285-361 MPa with a mean of 324 MPa. At high f_{O2}, some calculations repeatedly crashed, failing to return a result (n=6 at NNO +0.5, n=9 at NNO +1, n=24 at NNO +1.5).

The effect of f_{O2} on the plagioclase + orthopyroxene results

The equilibrium mineral assemblage results (and therefore pressure results) are sensitive to f_{O2} (Figure 5). In Figure 5a-d, we show geobarometry results for the same composition as Figure 2 but using different f_{O2} values. The input parameters for each calculation are identical except for f_{O2}. The effect of varying f_{O2} on the orthopyroxene saturation temperature is evident. At low f_{O2} (QFM -0.5), which results in lower Fe^{3+}/Fe^{total} in the melt, the orthopyroxene saturation temperature is high (Figure 5a). In this example, quartz is never in equilibrium with the measured melt composition. Therefore, the only acceptable pressure solution is plagioclase + orthopyroxene at 102 MPa. At more oxidizing f_{O2} and higher melt Fe^{3+}/Fe^{total} (Figure 6) the orthopyroxene saturates at lower temperatures. Because the orthopyroxene saturation temperature is lower, the plagioclase + orthopyroxene intersection occurs at higher pressures. This leads to a negative correlation between f_{O2} and plagioclase + orthopyroxene pressures (Figure 6). The relationship between f_{O2} and pressure is not linear (Figure 6), given that the Fe^{3+}/Fe^{total} ratio does not vary linearly with f_{O2}. For strongly reducing f_{O2} values (i.e., <<QFM or <<NNO, Figure 6), most of the iron in the system is reduced to Fe^{2+}. At strongly reducing f_{O2} the pressure values therefore become less dependent on f_{O2} (Figure 6). At more oxidizing f_{O2} (QFM +0.5, Figure 5c), the saturation temperature of orthopyroxene decreases, so the orthopyroxene saturation surface intersects with quartz and plagioclase on the liquidus. This means that it is possible for orthopyroxene, plagioclase, and quartz to be in equilibrium together with melt of the measured composition, resulting in a three-phase orthopyroxene + quartz + plagioclase pressure at 177 MPa. At even higher f_{O2} (QFM +1, Figure 5d), the orthopyroxene saturation temperature decreases further, such that the orthopyroxene saturation surface is below the quartz and plagioclase saturation surfaces. At this f_{O2}, orthopyroxene cannot be in equilibrium with quartz, plagioclase, and the measured melt composition. For this f_{O2}, the only acceptable pressure result is therefore quartz + plagioclase at 187 MPa. Importantly, the quartz + plagioclase pressure is the same as the three-phase orthopyroxene + quartz + plagioclase pressure, within the error of the parabola curve-fitting procedure (see Figure 2). In the cases in which quartz is not present, the quartz + plagioclase pressure represents a maximum pressure, given that only at pressures below that intersection can the melt of given composition be in equilibrium with plagioclase and not quartz – this result is independent of f_{O2}.

Discussion

Dealing with unknown f_{O2}

The strong dependence of orthopyroxene + plagioclase ± quartz pressures on f_{O2} (Figures 5 & 6) leads to a challenge: how do we constrain pressure for orthopyroxene-bearing dacites and rhyolites? Here, we discuss strategies for constraining pressure in the following scenarios: 1) we are confident that quartz is in equilibrium with the melt; 2) we are confident that quartz is NOT in equilibrium with the melt (but plagioclase and orthopyroxene are); 3) we are unsure if quartz is in equilibrium with the melt.

Scenario 1: quartz is in equilibrium with the melt

If we are confident that quartz is saturated, we can use the rhyolite-MELTS geobarometer to calculate the pressure of equilibration between the melt, quartz, and feldspar. For example, many of the TVZ rhyolites have plagioclase and quartz phenocrysts, which we are reasonably confident were in equilibrium with the surrounding melt (now quenched as glass) (Bégué, et al. 2014b; Gualda, et al. 2018; Smithies, et al. 2023). These quartz + plagioclase pressures are completely independent of f_{O2} – note that the quartz and plagioclase saturation surfaces shown in Figure 5 do not change with varying f_{O2}. Orthopyroxene is also a phenocryst phase in these rhyolites, so we could adjust f_{O2} to find a value that gives a quartz + plagioclase + orthopyroxene intersection. Importantly, the pressure of a three-phase intersection is the same as from the two-phase quartz + plagioclase intersection in the case where we adjust the f_{O2} to find the quartz + plagioclase + orthopyroxene intersection. The search in f_{O2} space therefore does not give us any further constraint on pressure, only on f_{O2}. This demonstrates that the quartz + feldspar geobarometer of Gualda and Ghiorso (2014) is sufficient to determine pressure in quartz-saturated systems without modelling additional phases. Nonetheless, quartz + plagioclase + orthopyroxene geobarometry could be used to find an f_{O2} that is internally consistent with the rhyolite-MELTS model.

Scenario 2: quartz is NOT in equilibrium with the melt

The rhyolites from the recent PCC eruptions have plagioclase and orthopyroxene phenocrysts, but quartz is absent (Table 1). This means that only a plagioclase + orthopyroxene ± clinopyroxene pressure solution would be acceptable. As the pyroxene saturation surfaces are

sensitive to f_{O2}, this makes constraining pressure more challenging. A first order approach is to use an f_{O2} value for the system that has been independently determined. Conveniently, the commonly used oxythermobarometer of Ghiorso and Evans (2008) is internally consistent with the MELTS family of thermodynamic models, so f_{O2} calculated with this oxythermobarometer are preferrable for finding pressures. For example, f_{O2} for the 2011 PCC eruption is estimated to be between NNO -0.9 and NNO -0.8 using the Ghiorso and Evans (2008) oxythermobarometer (Castro, et al. 2013; Jay, et al. 2014; Mingo 2019). The rhyolite-MELTS pyroxene + plagioclase pressure estimates at NNO -1.0 and NNO -0.75 for the 2011 PCC eruption (i.e., 25-146 MPa) are in excellent agreement with independent geobarometry and geophysical estimates of magma storage depths for the same eruption (50-140 MPa; Table 2) (Seropian, et al. 2021).

Even for eruptions where f_{O2} has not been determined, there is a limited range of f_{O2} that could be considered reasonable. Global compilations of erupted magmas from subduction systems show a limited range of f_{O2} between QFM and QFM +2.5 (Cottrell, et al. 2021; Ghiorso and Evans 2008; Ghiorso and Gualda 2013). The results from extremely reducing f_{O2} shown in Figure 6 are therefore generally implausible.

An important caveat to using f_{O2} constrained by Fe-Ti oxides is that we cannot be certain that the f_{O2} recorded by the Fe-Ti oxides was the f_{O2} of the system at the pressure recorded by the melt. Both Fe and Ti in Fe-Ti oxides can re-equilibrate rapidly (days) (Tomiya, et al. 2013; Van Orman and Crispin 2010), so they are likely to record the eruptive conditions and immediately prior to eruption rather than the longer-term pre-eruptive storage (years). During magma storage and ascent, f_{O2} is affected by complex open-system processes such as degassing (Burgisser and Scaillet 2007). If this is the case, the f_{O2} recorded by Fe-Ti oxides is not the f_{O2} of pre-eruptive storage. Using Fe-Ti oxides to estimate f_{O2} is particularly problematic for extraction pressures, as we consider the equilibration of the melt recorded by the bulk-rock, whereas the Fe-Ti oxide autocrysts likely equilibrated with the melt preserved as glass. (Figure 1).

In the absence of any information about f_{O2}, we make two crucial observations that can constrain a range of possible pressures. The first observation is that the plagioclase + orthopyroxene pressure must always be less than the quartz + plagioclase pressure, as

orthopyroxene must saturate at a higher temperature than quartz in quartz-undersaturated magma. Therefore, we can always constrain a maximum pressure in quartz-undersaturated magma by taking the quartz + plagioclase pressure to be the maximum. The second observation is that at strongly reducing f_{O2} values (e.g., <QFM -1.5, <NNO -1), as Fe^{3+}/Fe^{total} approaches 0, the orthopyroxene + plagioclase pressures approach a constant value (Figure 6). We can therefore also constrain a minimum pressure by calculating the pressure at strongly reducing conditions. These two observations give us a range of possible pressures. For some examples, this provides good constraint (e.g. between 94 and 187 MPa in Figure 6a), for others it gives broad constraint (e.g. between 144 and 345 MPa in Figure 6b). We note, however, that errors >100 MPa are typical for many commonly used mineral geobarometers (Wieser, et al. 2025; Wieser, et al. 2023b), thus this constraint is still somewhat informative.

Scenario 3: quartz may or may not be in equilibrium

There are several scenarios in which we are uncertain whether the system is quartz-saturated or not. Here, we show extraction pressures, in which we use whole-rock compositions from the TVZ to represent the theoretical melt that equilibrated with the mush mineral assemblage (Figure 1; Blundy 2022; Gualda, et al. 2019b). We are uncertain what mineral assemblage the melt was extracted from, as the mush typically does not erupt. Based on occasionally erupted mush fragments (Brown, et al. 1998; Burt, et al. 1998; Graeter, et al. 2015) and the composition of the erupted rhyolites, we can reasonably assume the mush in the TVZ is either granodioritic (plagioclase + quartz + orthopyroxene) or dioritic (plagioclase + orthopyroxene). This leaves us uncertain whether magmas erupted from the TVZ were extracted from a quartz-saturated or a quartz-undersaturated mush.

In cases in which we are uncertain of whether quartz is saturated or not, the quartz + plagioclase pressures are the maximum possible pressures (see Figure 5), with lower pressures possible with a plagioclase + orthopyroxene assemblage (Pamukçu, et al. 2021). This is also seen in Figure 4, which demonstrates that quartz + plagioclase pressures constitute a maximum bound on possible pressures. Figure 4 also shows that a range of orthopyroxene + plagioclase pressures is possible, depending on f_{O2}. If there is some information about f_{O2}, then the best estimate of f_{O2} for the system can be used to find both the likely pressure and the likely equilibrium mineral assemblage.

The PCC storage pressure results are only quartz-saturated at unreasonably high f_{O2} (>NNO +1), more than one log unit higher than the estimated f_{O2} for PCC (Figure 6). We would thus conclude – based on rhyolite-MELTS geobarometry – that PCC magmas are unlikely to be quartz-saturated. This agrees with observations of natural rocks, given that PCC volcanic rocks are typically quartz-absent (Table 1). In contrast, the rhyolite-MELTS models show that some of the TVZ melts extracted from the mush could have equilibrated with quartz at reasonable f_{O2} (Figure 6). This agrees with evidence from mush fragments co-erupted with TVZ rhyolites, some of which are quartz-bearing (Brown, et al. 1998; Burt, et al. 1998). In this sense, our results show that – at least in some cases – the rhyolite-MELTS geobarometer can be used to constrain mineral assemblage, which is particularly useful in the case of extraction pressures (see Gualda, et al. 2019b).

Plagioclase, orthopyroxene, and magnetite geobarometry

An alternative approach to solving the problem of the f_{O2} sensitivity of plagioclase + pyroxene geobarometry is to add a third phase to reduce the degrees of freedom. Although the PCC magmas are quartz-absent, the erupted rocks all have magnetite phenocrysts (Table 1). In Figure 7, we therefore plot the saturation surface of magnetite in addition to plagioclase and orthopyroxene. As a Fe-bearing phase, magnetite is also sensitive to f_{O2}. The saturation temperature of magnetite increases as f_{O2} increases, the inverse relationship to orthopyroxene. This inverse relationship is expected, given that magnetite has a higher partition coefficient for Fe^{3+} relative to Fe^{2+}, whereas orthopyroxene partitions Fe^{2+} more strongly. Therefore, it is possible to find a three-phase intersection of plagioclase + orthopyroxene + magnetite by incrementally adjusting f_{O2}. Magnetite is much more sensitive to f_{O2} than orthopyroxene, so smaller f_{O2} steps are necessary. From visual inspection of the example in Figure 7, the three-phase intersection must occur between NNO -1 and NNO -0.5. We therefore perform a binary search, first performing geobarometry calculations in 0.25 log intervals followed by 0.125 log intervals. We note, however, that rhyolite-MELTS is not precise to three decimal places so the significance of the second and third decimal places should not be overinterpreted. By performing this binary search, we find a three-phase intersection at NNO -0.75 for the composition shown in Figure 7.

To test this procedure, we search for plagioclase + orthopyroxene + magnetite intersections on every PCC composition. By visual inspection of the phase diagrams, we determine that the three-phase intersection must occur between NNO -1.25 and NNO for every composition (e.g., Figure 7). We therefore repeat the geobarometry calculations for each PCC composition at nine intervals between NNO -1.25 and NNO (i.e., 0.125 log steps), keeping all other model parameters the same (see Methods). Although inspection of the phase diagrams reveals three-phase intersections for most compositions (Figure 7), only 4 of the 33 compositions return a result using the parabola-fitting procedure shown in Figure 2. We therefore follow the methodology of Harmon, et al. (2018) and increase the residual temperature threshold to 10 °C. Because the magnetite saturation temperature is so sensitive to f_{O2}, a larger threshold is reasonable to avoid false negatives. With a 10 °C threshold, 24 of the 33 compositions return a result. Geobarometry results using a 5 °C, 8 °C, and 10 °C threshold are included in Online Resource 4. The overall pressure distribution is unchanged for the various thresholds used.

The plagioclase + orthopyroxene + magnetite pressures for the PCC samples are between 39 and 142 MPa, in excellent agreement with independent pressure estimates for PCC (Table 2; Figure 8). This suggests that the addition of magnetite improves the performance of the plagioclase + orthopyroxene geobarometer in quartz-absent magma and is an elegant solution to simultaneously constrain pressure and f_{O2}.

In addition, the f_{O2} at which these intersections occur (NNO -0.5 to NNO -1.125) mostly overlaps with f_{O2} estimated for the PCC magma using Fe-Ti oxides with the Ghiorso and Evans (2008) oxythermobarometer (NNO -0.1 to NNO -0.9, Figure 8). The Fe-Ti oxides suggest that the 1921-1922 had the most oxidizing conditions, 1960 was slightly more reducing, and 2011-2012 was much more reducing (Table 2). This trend is also apparent in the f_{O2} estimated with the plagioclase + orthopyroxene + magnetite geobarometer (Figure 8). This agreement is excellent given the errors associated with each method. It also suggests that, for PCC, the f_{O2} conditions recorded by the Fe-Ti oxides are very similar to the f_{O2} conditions recorded by the melt.

Comparison with independent melt geobarometers

To further test our method against independent geobarometers, we used the MagMaTaB melt geobarometer to calculate pressure for our compositions (Weber and Blundy 2024). MagMaTaB is a machine-learning based geothermobarometer that searches in P-T space from a database of experimental results. It requires a melt composition and the equilibrium mineral assemblage (presence-absence). For PCC storage pressures, we used the phenocryst assemblage (plagioclase + orthopyroxene + clinopyroxene + oxides; Table 1), assuming that this assemblage was in equilibrium with melt with composition equal to the glass composition. For the TVZ extraction pressures, we inferred the mush mineral assemblage from erupted mush fragments (plagioclase + orthopyroxene + hornblende + oxides ± quartz; Brown, et al. 1998). Erroneous quartz presence/absence skews MagMaTaB pressure results by ~200 MPa (Weber and Blundy 2024; their Figure 13), thus we repeat the extraction pressure calculations with and without quartz.

The MagMaTaB pressures are generally correlated with the rhyolite-MELTS pressures within the combined error of both methods (±80 MPa for MagMaTaB and ±20 to 80 MPa 2σ for rhyolite-MELTS), although MagMaTaB is consistently ~75-100 MPa higher than rhyolite-MELTS. For PCC, MagMaTaB pressures are ~100 MPa higher than both the rhyolite-MELTS pressures and the other independent geobarometry estimates for PCC summarized in Table 2. The TVZ results depend strongly on whether quartz is marked as present in the MagMaTaB calculation. For the compositions where rhyolite-MELTS predicted quartz undersaturation, there is good agreement between the rhyolite-MELTS and quartz-absent MagMaTaB results (Figure 9A). For the compositions where rhyolite-MELTS predicted quartz saturation, there is reasonable agreement with the quartz-present MagMaTaB results (Figure 9B). If we use rhyolite-MELTS to predict quartz saturation for the MagMaTaB calculation (Figure 9C), we achieve reasonable correlation between the models although the MagMaTaB pressures are 74 MPa higher on average.

This comparison demonstrates an important benefit of the rhyolite-MELTS modelling approach. Most melt geobarometers require a set mineral assemblage (Blundy 2022; Herzberg 2004; Voigt, et al. 2017; Wilke, et al. 2017; Yang, et al. 1996) or have mineral assemblage as a model input (Weber and Blundy 2024). The rhyolite-MELTS approach does

not require the equilibrium mineral assemblage to be known independently. For storage pressures, the autocrystic assemblage is only needed as a useful check of the model outputs. For extraction pressures where the mineral assemblage is unconstrained, the rhyolite-MELTS geobarometer makes it possible to both calculate pressure and infer mineral assemblage.

Importantly, inspection of the MagMaTaB calibrations presented by Weber and Blundy (2024) show that MagMaTaB pressures are generally overestimated for pressures <500 MPa, which – in combination with the systematic differences we observe here – suggests that rhyolite-MELTS pressures are both more precise and accurate than MagMaTaB pressures for shallow crustal magmas, particularly those that feed eruptions to the surface such as those studied here.

Implications and Conclusions

Quartz + plagioclase geobarometry as maximum pressure estimates

The most important implication of the relationships between quartz, feldspar, and orthopyroxene demonstrated in Figure 5 is that the maximum possible equilibration pressure of a rhyolite is given by the quartz + feldspar intersection, regardless of whether quartz is present in the system (Pamukçu, et al. 2021). At pressures higher than the quartz + feldspar equilibration pressure, feldspar is undersaturated, which is generally untenable for igneous rocks (e.g. Blundy and Cashman 2001; Gualda and Ghiorso 2013b).

The quartz + feldspar pressure results from rhyolite-MELTS have been repeatedly shown to compare well to other geobarometers (Al-in-hornblende and H_2O-CO_2 volatile saturation; Bégué, et al. 2014b; Gualda, et al. 2019a; Pamukçu, et al. 2015). The quartz + feldspar pressures are relatively insensitive to H_2O activity for shallow crustal magmas, particularly when they are fluid saturated (Ghiorso and Gualda 2015; Gualda and Ghiorso 2014), and, as shown in Figure 5, are insensitive to f_{O2}. Uncertainties on the quartz + feldspar geobarometer due to analytical uncertainties are on the order of 10-40 MPa 1σ, which depend on uncertainties associated with the used compositions (Gualda, et al. 2024; Gualda and Ghiorso 2014; Pamukçu, et al. 2021; Pitcher, et al. 2021; Smithies, et al. 2024; Smithies, et al. 2023). The quartz + feldspar geobarometer therefore provides a useful constraint on the

equilibration pressure of rhyolites, even in cases in which they are not quartz-saturated (see also Blundy and Cashman 2001; Gualda and Ghiorso 2013b; Harmon, et al. 2025; Ruefer, et al. 2025).

Estimating f_{O2}

A persistent challenge to plagioclase + pyroxene geobarometry is the sensitivity of the pressure results to f_{O2} (Harmon, et al. 2018). We show that this uncertainty can be reduced with two methods: 1) using independent estimates of f_{O2} (e.g., Fe-Ti oxides, assuming that the Fe-Ti oxides did not re-equilibrate during ascent) (Figure 6); and 2) searching in f_{O2} space for plagioclase + orthopyroxene + magnetite intersections (Figure 8). By adding magnetite, we can obtain more precise pressure estimates for quartz-absent systems, including systems where we have little independent information about f_{O2}. The success of the plagioclase + orthopyroxene + magnetite pressures is particularly important given that the pyroxene geobarometry results are sensitive to volatile concentrations, especially in volatile-undersaturated intermediate magma (Harmon, et al. 2018), and the pyroxene model in rhyolite-MELTS may not correctly predict the stability of clinopyroxene (see Brugman and Till 2019; Wieser, et al. 2025). The results shown in Figure 8 also demonstrate that it is possible to use the geobarometry procedure to obtain an estimate of f_{O2} from melt composition alone.

Beyond two- or three-phase rhyolite-MELTS geobarometers

In previous parts of this series (Bégué, et al. 2014b; Gualda and Ghiorso 2014; Harmon, et al. 2018; Pamukçu, et al. 2015) the quartz + feldspar, quartz + 2 feldspar, plagioclase + pyroxene, and the plagioclase + 2 pyroxene geobarometers were treated as separate entities. The methods that we have shown here, and the examples in Figures 2, 5, and 7, show how rhyolite-MELTS can be applied to search for the equilibration pressure between melt and any mineral assemblage of interest, within the constraints of the existing MELTS models.

Rhyolite-MELTS geobarometry does not need to be limited to just two or three mineral phases (Foley, et al. 2020; Gualda, et al. 2024). For example, Figure 10 shows a four-phase assemblage of quartz + plagioclase + orthopyroxene + magnetite for an extraction pressure calculation for a whole-rock composition from the TVZ. As with the three-phase plagioclase + orthopyroxene + magnetite calculations, we search in f_{O2} space for the intersections of multiple phases.

549 Although the example in Figure 10 does not give any further pressure information than a two-
550 phase assemblage, the multiple phase assemblage reduces the degrees of freedom in
551 compositional space and gives more confidence to the pressure calculation. If we are only
552 interested in pressure, searching in f_{O2} space for an orthopyroxene + quartz + plagioclase
553 solution does not provide further pressure information. Consequently, the quartz + feldspar
554 geobarometer of Gualda and Ghiorso (2014) is useful for magma saturated in quartz and
555 feldspar, without the need to add other phases (c.f. multiply saturated geobarometers, Blundy
556 2022). However, a multiple-phase solution has fewer degrees of freedom than a two-phase
557 solution, so three- or four- phase pressure results will have smaller uncertainties resulting
558 from analytical precision (Gualda and Ghiorso 2014; Pamukçu, et al. 2021; Pitcher, et al. 2021;
559 Smithies, et al. 2024; Smithies, et al. 2023).

560 Searching for relevant multiple phase intersections could refine uncertain melt compositions
561 and intensive parameters (Harmon, et al. 2025). In the examples presented here, we have
562 shown that three-phase intersections that include Fe-bearing phases are useful for refining
563 f_{O2}. Further, it would be informative to probe other parameters, for example adjusting volatile
564 content or major-element compositions within uncertainty. When the melt composition is
565 known, the coincidence of four or more phases increases our confidence that – in some cases
566 – the geobarometer can be used to infer likely mineral assemblages. The Rhyolite-MELTS
567 geobarometer is useful for more than just pressure when information from multiple phases is
568 investigated.

569 Rhyolite-MELTS geobarometry does not need to be limited to three phases, and multiple
570 saturation of a higher number of phases can (1) give further constraints on intensive
571 parameters; (2) yield pressure estimates with smaller uncertainties; and (3) help determine
572 mineral assemblages that equilibrated with a given melt composition. We demonstrate how
573 rhyolite-MELTS can be used to search for equilibration pressures between melt and any
574 mineral assemblage of interest (within the limitations of rhyolite-MELTS), and give examples
575 of quartz, plagioclase, orthopyroxene, and magnetite. We hope this paper can be a guide to
576 interpretation of rhyolite-MELTS results that move beyond the established geobarometry
577 applications.

This is a preprint submitted to EarthArXiv. This manuscript has been peer-reviewed and is in revision in Contributions to Minerology and Petrology.

Authorship contribution statement

All authors contributed to the study conception. Smithies performed the data analysis, wrote the first draft of the manuscript, and drafted the figures. All authors commented on and revised subsequent versions of the manuscript.

Competing interests

No funding was received to assist with the preparation of this manuscript. The authors have no relevant financial or non-financial interests to disclose.

Acknowledgements

We thank Jon Blundy and Rebecca Lange for their thoughtful and constructive reviews, and Gordon Moore for editorial handling. Smithies and Harmon thank Gilles Seropian for introducing us to the Puyehue-Cordón Caulle system and for sharing the rhyolite-MELTS data from his previous work.

Supplementary information

Online Resource 1: Spreadsheet of compositions used in this study with geobarometry results.

Online Resource 2: Animated version of Figure 5 showing orthopyroxene saturation surface temperature decreasing as f_{O2} increases.

Online Resource 3: Animated version of Figure 7 showing magnetite saturation surface temperature increasing as f_{O2} increases.

Online Resource 4: Plagioclase + orthopyroxene + magnetite geobarometry results for PCC as in Figure 8 calculated with a residual temperature threshold of ≤8 °C and ≤5 °C.

Tables

Table 1 Characteristics of the eruptions included in this study.

Volcanic center	Eruption	Eruption age	Volume (km^3)	Phenocryst assemblage	Crystal content	f_{O2}
Taupō Volcanic Zone (TVZ), Aotearoa New Zealand	Mamaku	240 ± 11 ka[a]	100	Plagioclase > quartz > orthopyroxene + Fe-Ti oxides > ± tr. augite ± tr. hornblende [d]	5-7 vol.% [d]	QFM 0 to +0.8 [j]
	Ohakuri	240 ± 11 ka[b]	150	Plagioclase > quartz > orthopyroxene > Fe-Ti oxides [e]	<5 vol.% [e]	QFM 0 to +0.8 [j]
	Pokai	275 ± 20 ka[a]	100	Plagioclase > orthopyroxene > quartz > Fe-Ti oxides > ± tr. clinopyroxene ± tr. amphibole [f]	2-8 vol.% [f]	QFM -0.2 to +0.6 [k, l]
	Kaingaroa	298 ± 3 ka[c]	100	Plagioclase > orthopyroxene > Fe-Ti oxides > ± tr. hornblende ± tr. augite ± tr. quartz [g]	<3.5 wt.% [g]	QFM 0 to +0.4 [m]
	Chimp	ca. 310 ka	50	Plagioclase > orthopyroxene + Fe-Ti oxides > > ± amphibole ± tr. clinopyroxene ± tr. quartz ± tr. biotite	<8 vol.% [f]	QFM +0.3 [l]
Puyehue-Cordón Caulle (PCC), Chile	1921-1922 (CCV)	1921-1922 CE	0.4	Plagioclase + orthopyroxene + clinopyroxene + spinel [h]	5-15% [h]	NNO -0.4 to -0.1 [n, o]
	1960 (CCVI)	1960 CE	0.25	Plagioclase + orthopyroxene + clinopyroxene + spinel [h]	5-15% [h]	NNO -0.5 to -0.2 [n, o]
	2011-2012	2011-2012 CE	1.5	plagioclase > orthopyroxene > clinopyroxene > magnetite + ilmenite [i]	5 vol.% [i]	NNO -0.9 to -0.8 [o, p, q]

Age references: a) Leonard (2003); b) Gravley, et al. (2007); c) Downs, et al. (2014).

602 Petrography references: d) Milner, et al. (2003); e) Gravley (2004); f) Karhunen (1993); g)
603 Beresford, et al. (2000); h) Gerlach, et al. (1988) i) Castro, et al. (2013).

604 f_{O2} references, all calculated with the oxythermobarometer of Ghiorso and Evans (2008): j)
605 Bégué, et al. (2014a) k) recalculated from oxide compositions reported by Deering, et al.
606 (2010); l) recalculated from oxide compositions reported by Karhunen (1993); m) recalculated
607 from oxide compositions reported by Beresford, et al. (2000); n) Gerlach, et al. (1988); o)
608 Mingo (2019); p) Castro, et al. (2013); q) Jay, et al. (2014).

609

610

611 **Table 2** Comparison of pre-eruptive storage pressure estimates for the 2011 PCC eruption
612 using independent petrologic and geophysical techniques.

Pressure estimate method	H_2O-CO_2 geobarometer*	Petrologic experiments	Inflation source modelled from InSAR⁺	Rhyolite-MELTS plagioclase + pyroxene geobarometer at ΔNNO -1.0	Rhyolite-MELTS plagioclase + pyroxene geobarometer at ΔNNO -0.75	Rhyolite-MELTS plagioclase + pyroxene + magnetite geobarometer	MagMaTaB
	Jay, et al. (2014)	Castro, et al. (2013)	Delgado, et al. (2019); Jay, et al. (2014); Wendt, et al. (2017)	Seropian, et al. (2021); this study	Seropian, et al. (2021); this study	This study	This study
P_{min}		50	90	25	49	39	89
P_{mean}	140			73	90	76	187
P_{max}		115	135	123	146	142	239

613 *In pyroxene glass inclusions (n=6) using the H_2O-CO_2 model of Papale, et al. (2006)
614 ⁺Converted from depth assuming a crustal density of 2.3 g cm^{-3}.

Figures

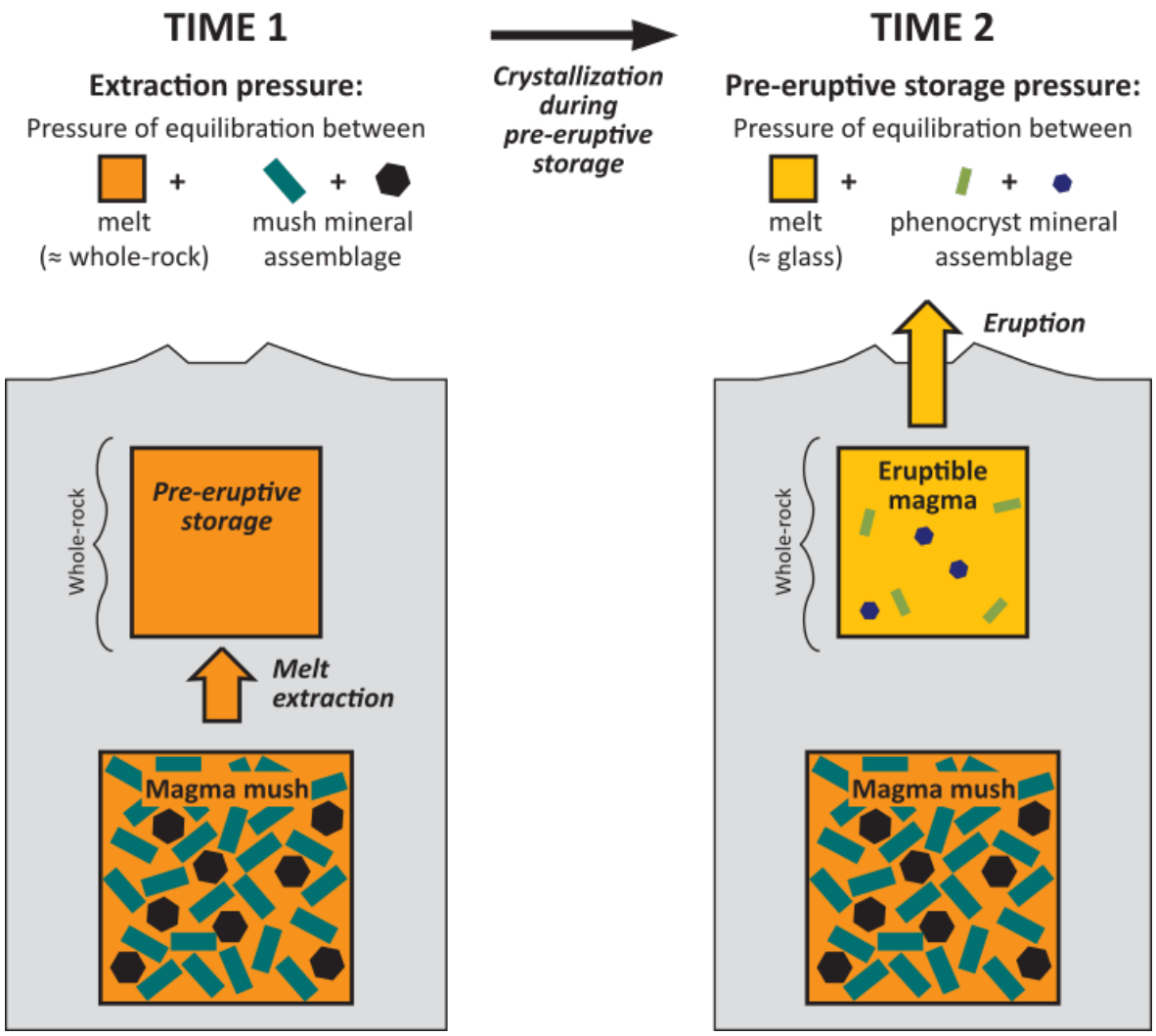

Fig. 1 Conceptual magma system model after Gualda, et al. (2019b) showing definition of extraction pressure (equilibration between bulk magma composition and the mush mineral assemblage) and pre-eruptive storage pressure (equilibration between melt and crystals immediately prior to eruption). In the case of extraction pressures, the mush mineral assemblage is unknown, whilst in the case of storage pressures the phenocrysts could be assumed to be in equilibrium with the glass composition.

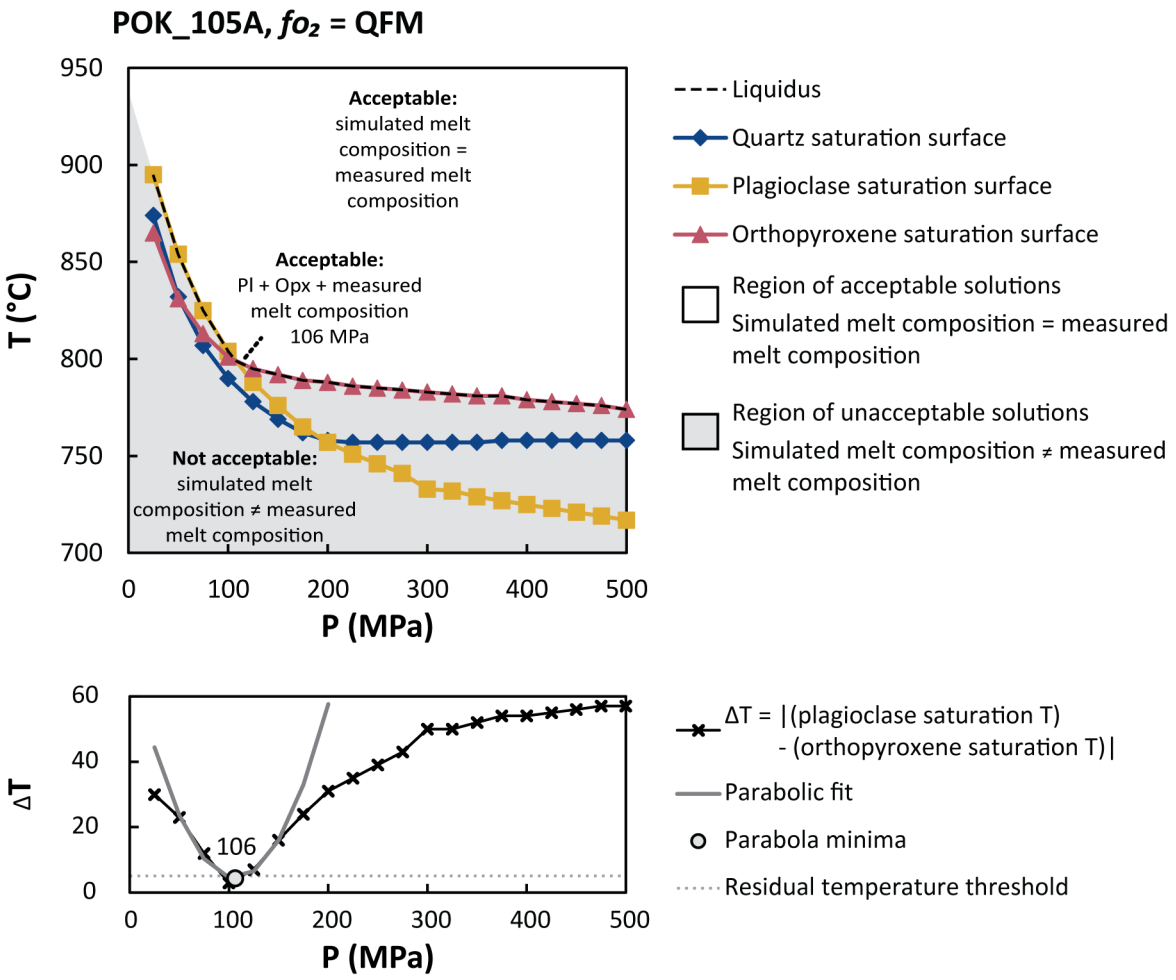

Fig. 2 Top: pressure-temperature phase diagram result from a typical rhyolite-MELTS geobarometry calculation (sample POK_105A at the QFM buffer). Above the liquidus (dashed line) the melt composition simulated by rhyolite-MELTS is the same as the bulk composition of the system input by the user (i.e. the measured composition, a whole-rock pumice composition in this case). Below the liquidus, the simulated melt is fractionated, so the simulated melt does not have the same composition as the measured melt composition. This means that pressure solutions for the measured melt composition must be on or above the liquidus. If both plagioclase and orthopyroxene are in equilibrium with the measured melt composition, the only possible pressure is at the intersection of the plagioclase and orthopyroxene saturation surfaces at 106 MPa. Bottom: illustration of parabola-fitting procedure to determine the pressure that the plagioclase and orthopyroxene saturation surfaces intersect. A parabola is fit along the lowest temperature difference and the temperature differences two pressure steps either side of the lowest temperature difference.

639 The parabola-fitting procedure is only performed if $\Delta T \leq 5$ °C (the residual temperature
640 threshold). This ensures that pressures are only calculated if there is a true intersection.

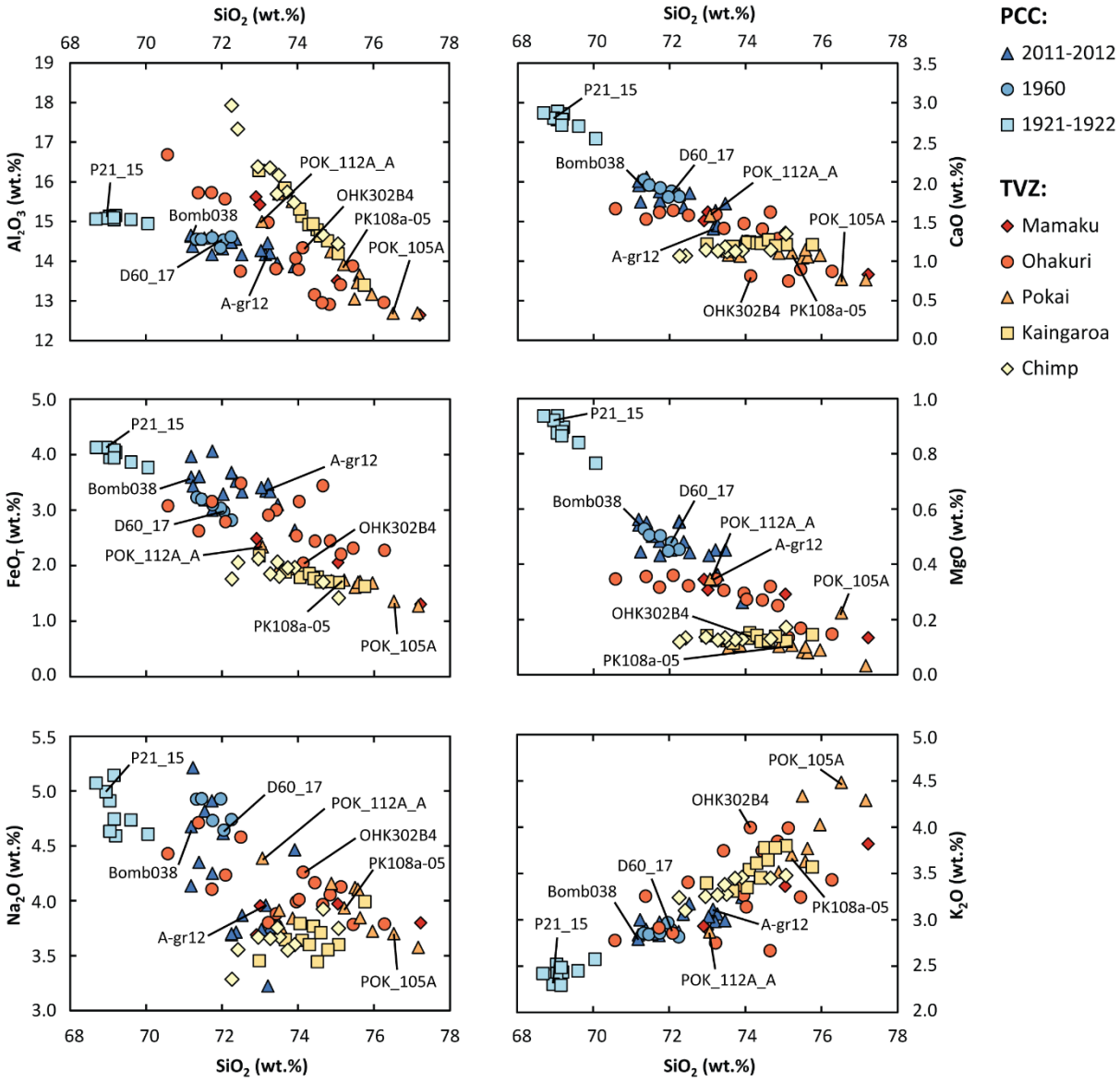

Fig. 3 Major-element compositions from PCC (blue symbols) and TVZ (yellow-red symbols) samples used for the geobarometry calculations in this study. Compositions used as examples in Figures 2, 5, 6, 7, and 9 are labelled. All compositional data is included in Online Resource 1.

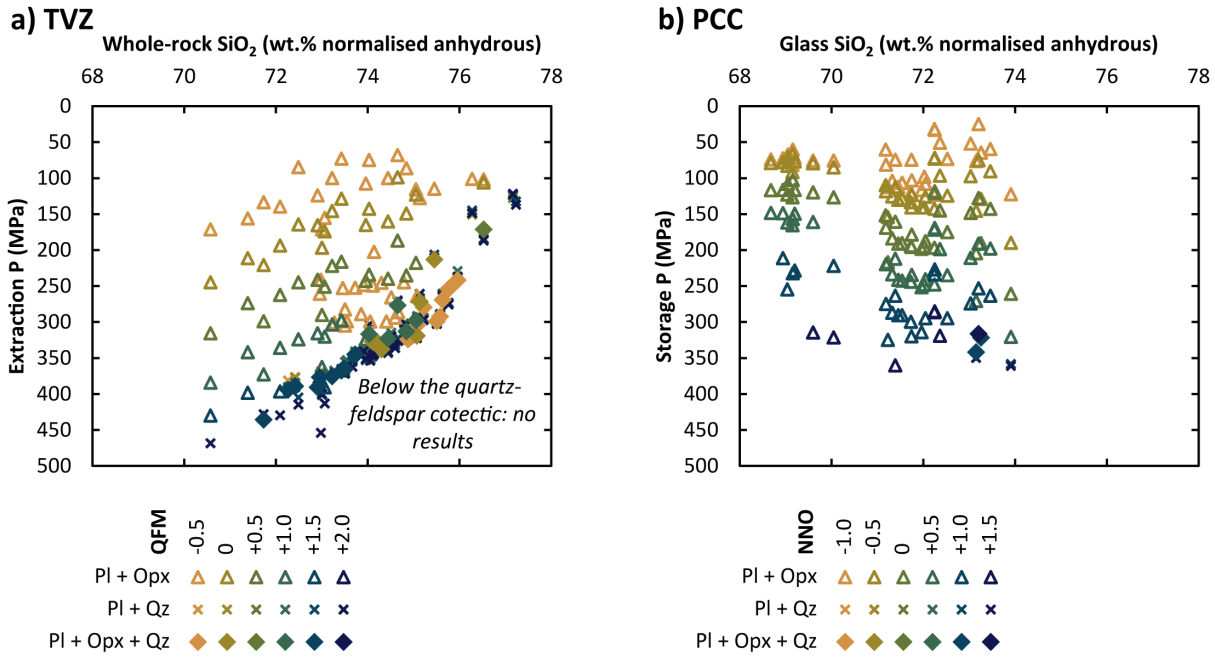

Fig. 4 Geobarometry results for all compositions at various f_{O2} (Online Resource 1). Symbol shape shows acceptable mineral assemblage as in Figure 6, symbol shading shows f_{O2} as in Figure 6. In the high-silica rhyolites of the TVZ (a) there is a region below the quartz-feldspar cotectic where no pressure solutions are possible. This demonstrates that the quartz + feldspar geobarometer can be used to constrain maximum pressure.

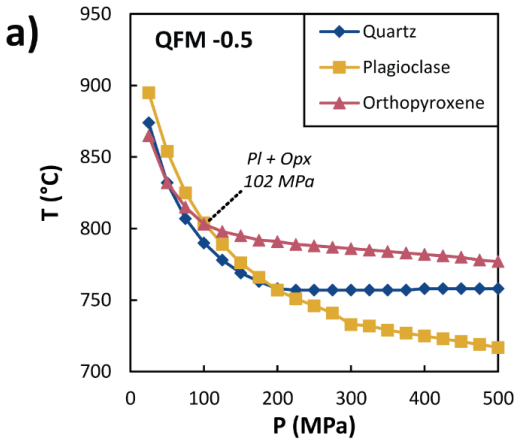
a)
QFM -0.5
Quartz
Plagioclase
Orthopyroxene
Pl + Opx
102 MPa
T (°C)
P (MPa)

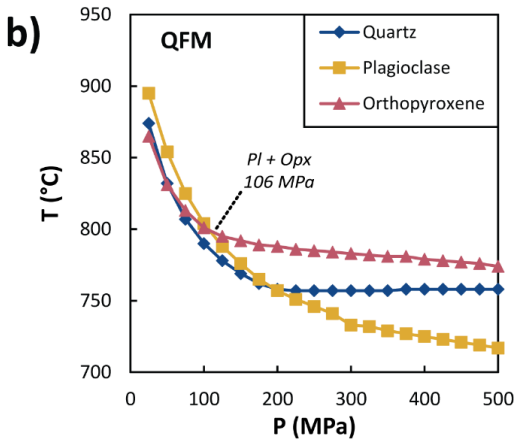
b)
QFM
Quartz
Plagioclase
Orthopyroxene
Pl + Opx
106 MPa
T (°C)
P (MPa)

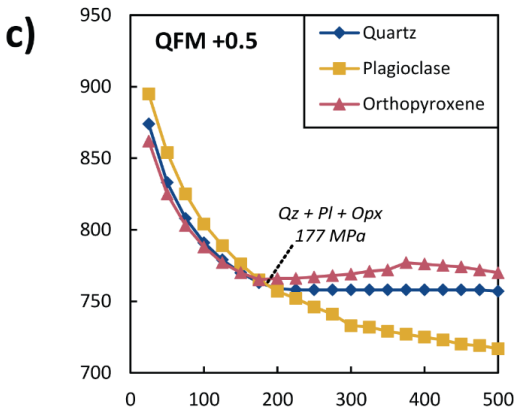
c)
QFM +0.5
Quartz
Plagioclase
Orthopyroxene
Qz + Pl + Opx
177 MPa
T (°C)
P (MPa)

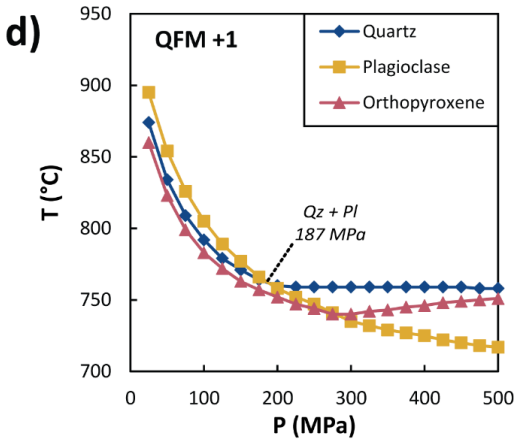
d)
QFM +1
Quartz
Plagioclase
Orthopyroxene
Qz + Pl
187 MPa
T (°C)
P (MPa)

654

Fig. 5 Example of quartz + plagioclase + orthopyroxene saturation surfaces for the same model inputs (sample POK_105A) but with different f_{O2} values for each panel. The quartz and plagioclase saturation temperatures and pressures do not vary with f_{O2}, whilst the orthopyroxene saturation temperature decreases as f_{O2} increases. At low f_{O2} (QFM -0.5 and 0; a, b) the only acceptable pressure results are plagioclase + orthopyroxene. At moderate f_{O2} (QFM +0.5; c) there is a three-phase plagioclase + orthopyroxene + quartz pressure solution. At high f_{O2} (QFM +1; d) orthopyroxene is no longer saturated on the liquidus so only quartz + plagioclase pressure solutions are possible. An animated version of this figure showing an extended range of f_{O2} is available in Online Resource 2.

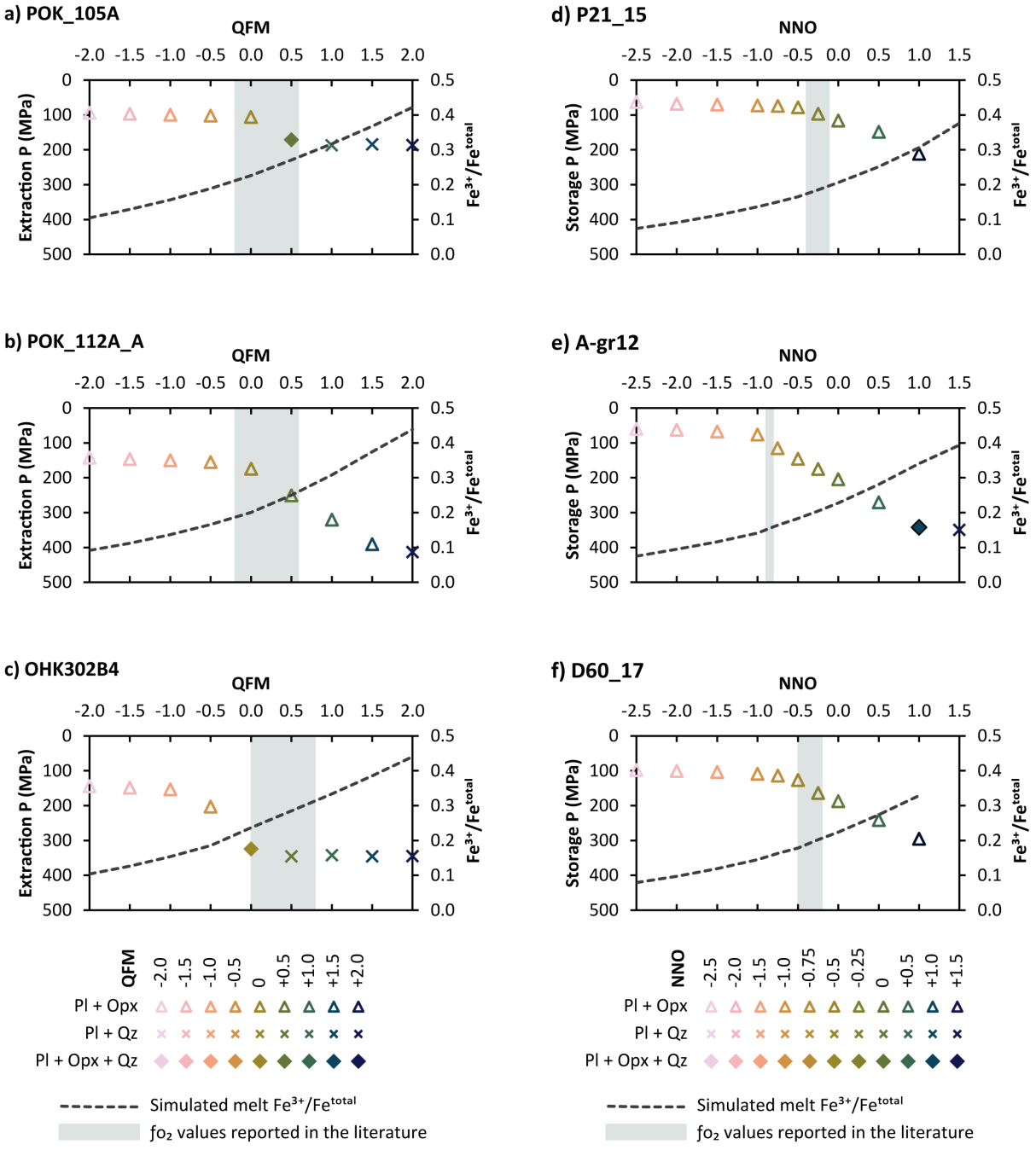

Fig. 6 Three examples of geobarometry results from the TVZ (a-c) and PCC (d-f) as a function of f_{O2}. Note that a) shows the same calculations as Figure 5. Symbol shape shows acceptable mineral assemblage as in Figure 4, symbol shading shows f_{O2} as in Figure 4. Acceptable mineral assemblage shown with symbols. At low f_{O2} the results are plagioclase + orthopyroxene (triangles), as f_{O2} increases some compositions return quartz + plagioclase + orthopyroxene (diamonds), and at high f_{O2} some compositions return quartz + plagioclase (x's). The dashed line shows Fe^{3+}/Fe^{total} in the simulated liquid modelled by rhyolite-MELTS. This is correlated

673 with f_{O2}, leading to the sensitivity of pyroxene to f_{O2}. The grey boxes show the range of f_{O2}

674 reported for that eruption based on Fe-Ti oxides (see Table 1).

675

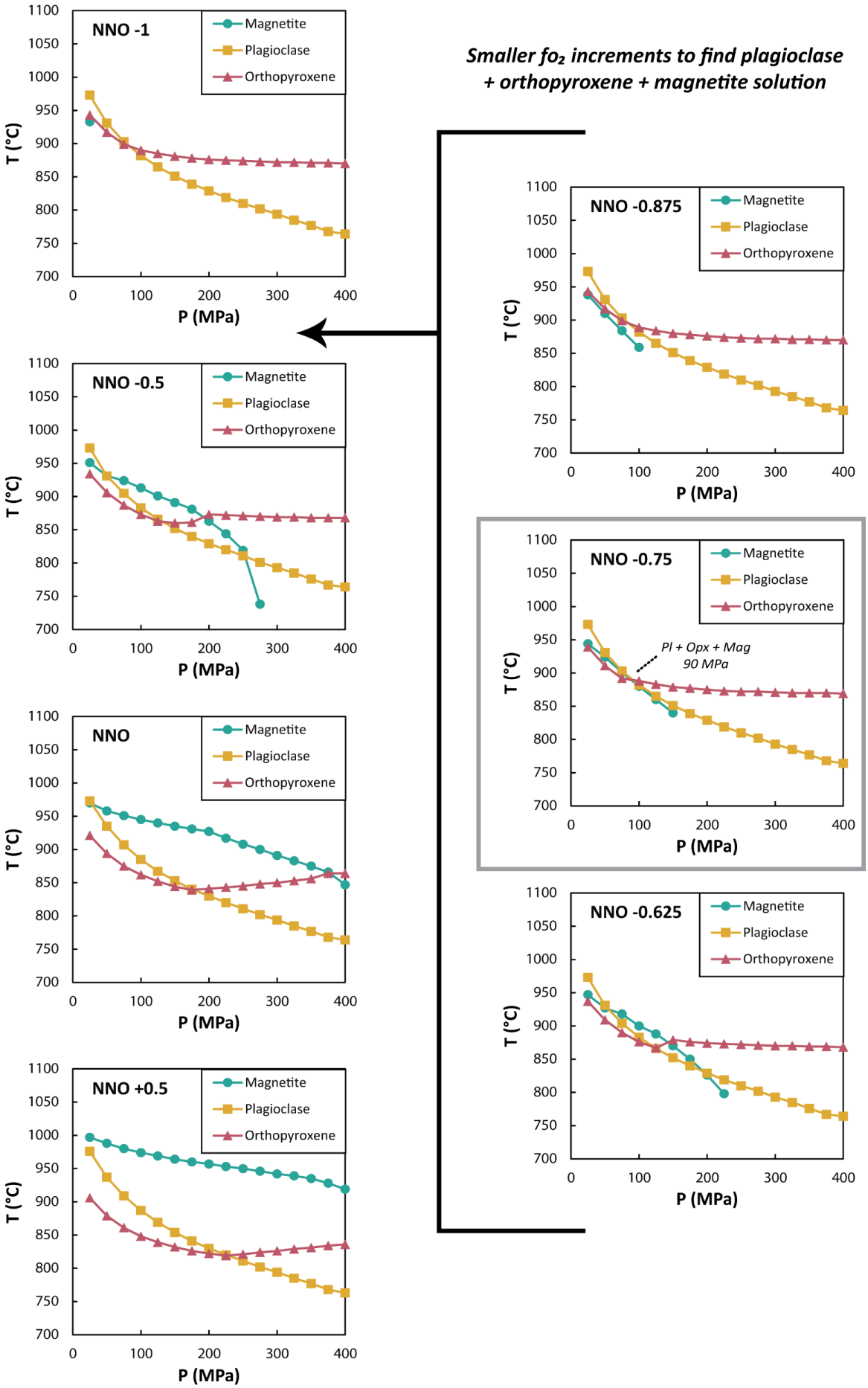

Fig. 7 Example of plagioclase + orthopyroxene + magnetite saturation surface intersections at varying f_{O2} (sample Bomb038, PCC). The left column shows calculations performed at 0.5 log interval f_{O2} steps. The orthopyroxene saturation temperature moves down as f_{O2} increases, conversely, magnetite saturation temperature moves up as f_{O2} increases. This means it is possible to find a three-phase intersection by adjusting f_{O2}. As magnetite is very sensitive to f_{O2}, small increments are necessary. In this example, the three-phase intersection must occur between NNO -1 and NNO -0.5 (arrow). The right column shows small 0.125 log increment f_{O2} steps within this interval. A three-phase solution is found at NNO -0.75, giving a three-phase pressure of 90 MPa. An animated version of this figure showing saturation surfaces moving with f_{O2} is available in the Online Resource 3.

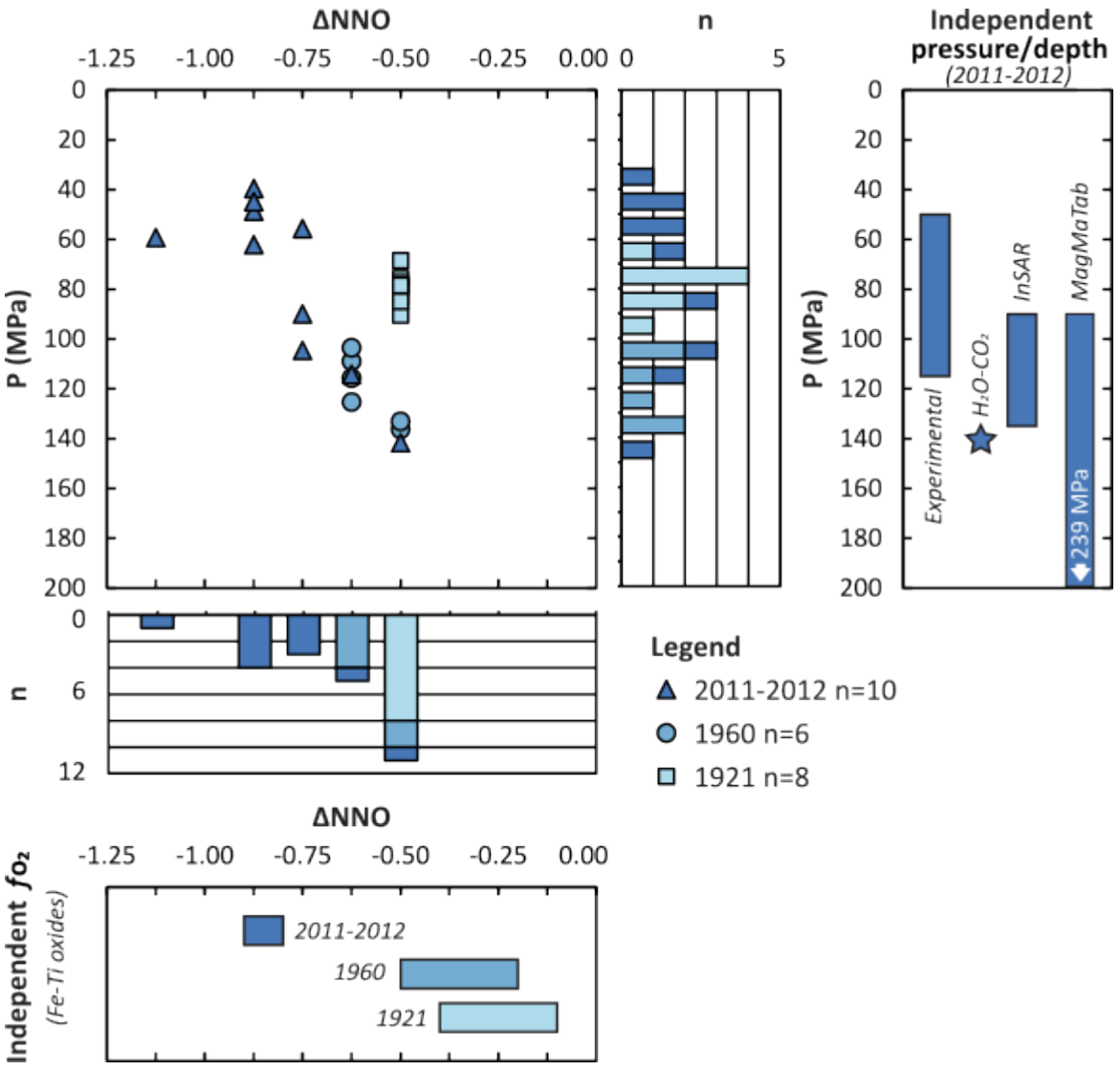

Fig. 8 Plagioclase + orthopyroxene + magnetite geobarometry results for PCC compositions, showing both the pressure result and the f_{O2} at which the three-phase intersection occurred. Results are calculated with a residual temperature threshold of ≤10 °C, see Online Resource 4 for results with ≤8 °C and ≤5 °C thresholds. Our results are compared to independently estimated pressure for the 2011-2012 eruption (see Table 2) and f_{O2} estimated from Fe-Ti oxides for each eruption as reported in the literature (see Table 1). Depth from InSAR studies is converted to pressure, assuming a crustal density of 2.3 g cm^{-3}. Boxes indicate range (maximum-minimum), star indicates a mean value. There is excellent agreement between these independent P and f_{O2} estimates and both the P and f_{O2} results of the plagioclase + orthopyroxene + magnetite geobarometer.

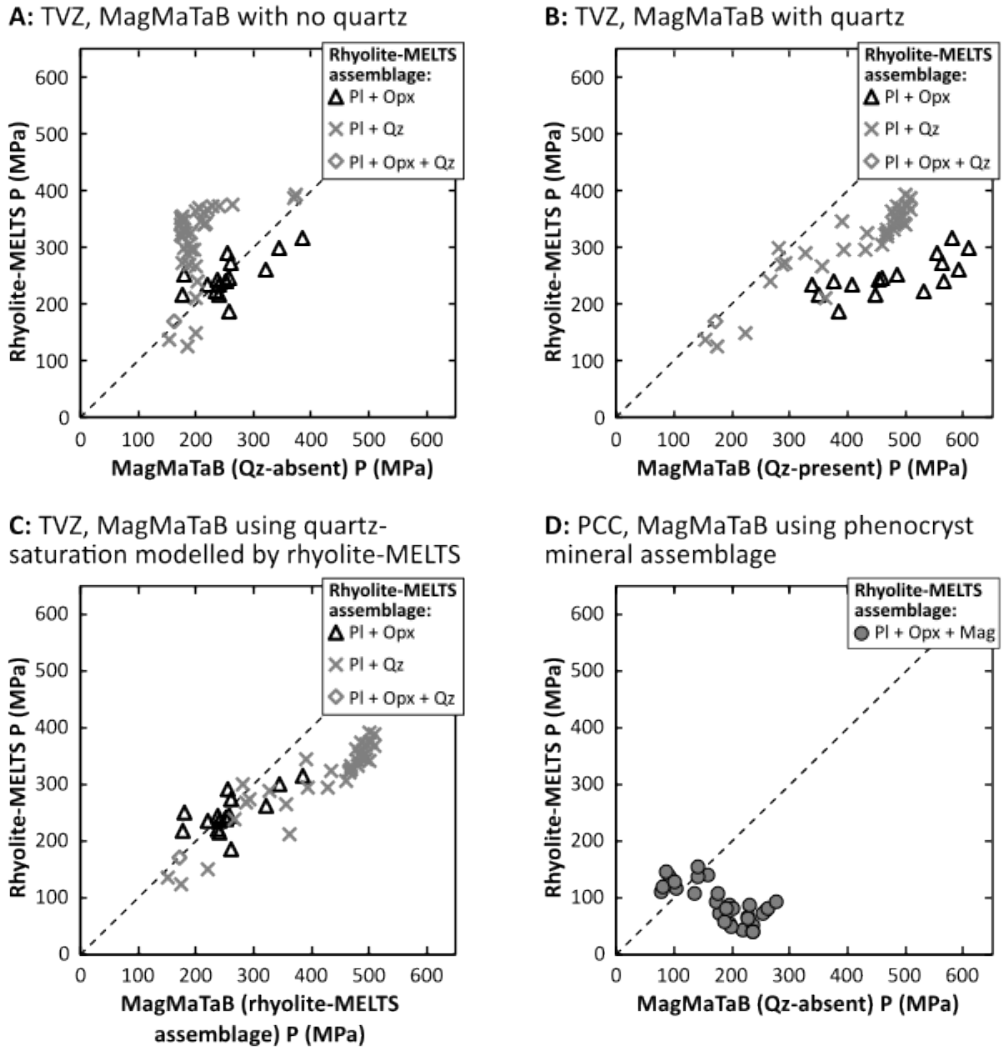

Fig 9 Comparison between rhyolite-MELTS geobarometry results presented here and MagMaTaB results (Weber and Blundy 2024). Panels A-C show extraction pressure results for the TVZ. Rhyolite-MELTS calculations are all run at QFM +0.5, symbols show mineral assemblage predicted by rhyolite-MELTS. The MagMaTaB pressure results are sensitive to quartz presence or absence in the model input. The quartz-absent (panel A) results agree well with the quartz-absent plagioclase + orthopyroxene results from rhyolite-MELTS, the quartz-present (panel B) agree well with the rhyolite-MELTS plagioclase + quartz ± orthopyroxene results. Using the rhyolite-MELTS results to inform quartz presence or absence in MagMaTaB (panel C), we find reasonable agreement between the models. Panel D shows MagMaTaB results for PCC glass compositions calculated with the phenocryst assemblage (Table 1) compared to rhyolite-MELTS plagioclase + orthopyroxene + magnetite results.

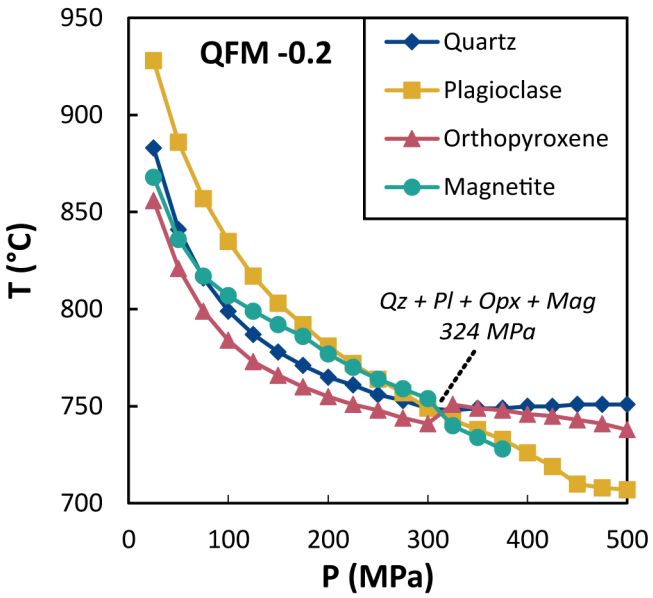

Fig. 10 Examples of a four-phase intersection (plagioclase + quartz + orthopyroxene + magnetite) from sample PK108a-05 (Pokai eruption, TVZ) at QFM -0.2. This intersection does not provide any further pressure constraint than a two- or three-phase intersection, but by reducing the degrees of freedom we can constrain f_{O2} (QFM -0.2) and the likely mineral assemblage (quartz-bearing in this example).

References

Anderson Jr AT, Newman S, Williams SN, Druitt TH, Skirius C, Stolper E (1989) H2O, CO2, Cl, and gas in Plinian and ash-flow Bishop rhyolite. Geology 17(3):221-225

Bachmann O, Dungan MA, Lipman PW (2002) The Fish Canyon Magma Body, San Juan Volcanic Field, Colorado: Rejuvenation and Eruption of an Upper-Crustal Batholith. J Petrol 43(8):1469-1503 doi:10.1093/petrology/43.8.1469

Bégué F, Deering CD, Gravley DM, Kennedy BM, Chambefort I, Gualda GAR, Bachmann O (2014a) Extraction, storage and eruption of multiple isolated magma batches in the paired Mamaku and Ohakuri eruption, Taupo Volcanic Zone, New Zealand. J Petrol 55(8):1653-1684 doi:10.1093/petrology/egu038

Bégué F, Gualda GAR, Ghiorso MS, Pamukçu AS, Kennedy BM, Gravley DM, . . . Chambefort I (2014b) Phase-equilibrium geobarometers for silicic rocks based on rhyolite-MELTS. Part 2: application to Taupo Volcanic Zone rhyolites. Contrib Mineral Petrol 168(5):1-16 doi:10.1007/s00410-014-1082-7

Beresford SW, Cole JW, Weaver SD (2000) Weak chemical and mineralogical zonation in the Kaingaroa Ignimbrite, Taupo volcanic zone, New Zealand. New Zealand Journal of Geology and Geophysics 43(4):639-650 doi:10.1080/00288306.2000.9514914

Black BA, Andrews BJ (2020) Petrologic imaging of the architecture of magma reservoirs feeding caldera-forming eruptions. Earth Planet Sci Lett 552 doi:10.1016/j.epsl.2020.116572

Blundy J (2022) Chemical Differentiation by Mineralogical Buffering in Crustal Hot Zones. J Petrol 63(7):egac054

Blundy J, Cashman K (2001) Ascent-driven crystallisation of dacite magmas at Mount St Helens, 1980–1986. Contrib Mineral Petrol 140(6):631-650

Brown SJA, Burt RM, Cole JW, Krippner SJP, Price RC, Cartwright I (1998) Plutonic lithics in ignimbrites of Taupo Volcanic Zone, New Zealand; sources and conditions of crystallisation. Chemical Geology 148(1):21-41 doi:10.1016/S0009-2541(98)00026-6

Brugman KK, Till CB (2019) A low-aluminum clinopyroxene-liquid geothermometer for high-silica magmatic systems. American Mineralogist 104(7):996-1004 doi:10.2138/am-2019-6842

Burgisser A, Scaillet B (2007) Redox evolution of a degassing magma rising to the surface. Nature 445(7124):194-197

Burnham CW (1994) Development of the Burnham model for prediction of H2O solubility in magmas. In: Volatiles in magmas, vol 30. De Gruyter, pp 123-130

Burt RM, Brown SJA, Cole JW, Shelley D, Waight TE (1998) Glass-bearing plutonic fragments from ignimbrites of the Okataina caldera complex, Taupo Volcanic Zone, New Zealand: remnants of a

752 partially molten intrusion associated with preceding eruptions. J Volcanol Geotherm Res 84(3):209-
753 237 doi:10.1016/S0377-0273(98)00039-0

754 Caricchi L, Townsend M, Rivalta E, Namiki A (2021) The build-up and triggers of volcanic eruptions.
755 Nature Reviews Earth & Environment:1-19

756 Castro JM, Schipper CI, Mueller SP, Militzer AS, Amigo A, Parejas CS, Jacob DE (2013) Storage and
757 eruption of near-liquidus rhyolite magma at Cordon Caulle, Chile. Bulletin of Volcanology 75(4):1-17
758 doi:10.1007/s00445-013-0702-9

759 Cooper GF, Wilson CJN, Millet M-A, Baker JA, Smith EGC (2012) Systematic tapping of independent
760 magma chambers during the 1 Ma Kidnappers supereruption. Earth Planet Sci Lett 313:23-33
761 doi:10.1016/j.epsl.2011.11.006

762 Cottrell E, Birner SK, Brounce M, Davis FA, Waters LE, Kelley KA (2021) Oxygen fugacity across tectonic
763 settings. Magma redox geochemistry:33-61

764 Deering CD, Gravley DM, Vogel TA, Cole JW, Leonard GS (2010) Origins of cold-wet-oxidizing to hot-dry-
765 reducing rhyolite magma cycles and distribution in the Taupo Volcanic Zone, New Zealand. Contrib
766 Mineral Petrol 160(4):609-629 doi:10.1007/s00410-010-0496-0

767 Delgado F, Kubanek J, Anderson K, Lundgren P, Pritchard M (2019) Physicochemical models of effusive
768 rhyolitic eruptions constrained with InSAR and DEM data: A case study of the 2011-2012 Cordón Caulle
769 eruption. Earth Planet Sci Lett 524:115736

770 Downs DT, Rowland JV, Wilson CJN, Rosenberg MD, Leonard GS, Calvert AT (2014) Evolution of the
771 intra-arc Taupo-Reporoa basin within the Taupo volcanic zone of New Zealand. 10(1):185-206
772 doi:10.1130/GES00965.1

773 Edmonds M, Cashman KV, Holness M, Jackson M (2019) Architecture and dynamics of magma
774 reservoirs. Philosophical Transactions of the Royal Society of London Series A: Mathematical, Physical,
775 and Engineering Sciences 377(2139):20180298-20180298 doi:10.1098/rsta.2018.0298

776 Foley ML, Miller CF, Gualda GAR (2020) Architecture of a super-sized magma chamber and
777 remobilization of its basal cumulate (Peach Spring Tuff, USA). J Petrol 61(1)
778 doi:10.1093/petrology/egaa020

779 Gerlach DC, Frey FA, Moreno-Roa H, Lopez-Escobar L (1988) Recent volcanism in the Puyehue—Cordon
780 Caulle region, Southern Andes, Chile (40· 5° S): petrogenesis of evolved lavas. J Petrol 29(2):333-382

781 Ghiorso MS, Evans BW (2008) Thermodynamics of rhombohedral oxide solid solutions and a revision
782 of the Fe-Ti two-oxide geothermometer and oxygen-barometer. American Journal of Science
783 308(9):957-1039

784 Ghiorso MS, Gualda GAR (2013) A method for estimating the activity of titania in magmatic liquids
785 from the compositions of coexisting rhombohedral and cubic iron–titanium oxides. Contrib Mineral
786 Petrol 165(1):73-81 doi:10.1007/s00410-012-0792-y

787 Ghiorso MS, Gualda GAR (2015) An H2O–CO2 mixed fluid saturation model compatible with rhyolite-
788 MELTS. Contrib Mineral Petrol 169(6):1-30 doi:10.1007/s00410-015-1141-8

789 Giordano G, Caricchi L (2022) Determining the State of Activity of Transcrustal Magmatic Systems and
790 Their Volcanoes. Annu Rev Earth Planet Sci Lett 50(1):231-259 doi:10.1146/annurev-earth-032320-
791 084733

792 Gonnermann HM, Manga M (2007) The fluid mechanics inside a volcano. Annu Rev Fluid Mech
793 39(1):321-356

794 Graeter KA, Beane RJ, Deering CD, Gravley D, Bachmann O (2015) Formation of rhyolite at the Okataina
795 volcanic complex, New Zealand; new insights from analysis of quartz clusters in plutonic lithics. Am
796 Mineral 100(8-9):1778-1789 doi:10.2138/am-2015-5135

797 Gravley DM (2004) The Ohakuri pyroclastic deposits and the evolution of the Rotorua-Ohakuri
798 volcanotectonic depression. PhD. University of Canterbury

799 Gravley DM, Wilson CJN, Leonard GS, Cole JW (2007) Double trouble: Paired ignimbrite eruptions and
800 collateral subsidence in the Taupo Volcanic Zone, New Zealand. Bulletin of the Geological Society of
801 America 119(1-2):18-30 doi:10.1130/B25924.1

802 Gualda GA, Miller CF, Wallrich BM (2024) The rhyolite factory: insights from rhyolite-MELTS
803 geobarometry of plutonic rocks and associated volcanics. J Petrol 65(12):egae123

804 Gualda GAR, Bégué F, Pamukçu AS, Ghiorso MS (2019a) Rhyolite-MELTS vs DERP—Newer Does not
805 Make it Better: a Comment on 'The Effect of Anorthite Content and Water on Quartz–Feldspar Cotectic
806 Compositions in the Rhyolitic System and Implications for Geobarometry' by Wilke et al. (2017; Journal
807 of Petrology, 58, 789–818). J Petrol 60(4):855-864 doi:10.1093/petrology/egz003

808 Gualda GAR, Ghiorso MS (2013a) The Bishop Tuff giant magma body: an alternative to the Standard
809 Model. Contrib Mineral Petrol 166(3):755-775 doi:10.1007/s00410-013-0901-6

810 Gualda GAR, Ghiorso MS (2013b) Low-Pressure Origin of High-Silica Rhyolites and Granites. The Journal
811 of Geology 121(5):537-545 doi:10.1086/671395

812 Gualda GAR, Ghiorso MS (2014) Phase-equilibrium geobarometers for silicic rocks based on rhyolite-
813 MELTS. Part 1: Principles, procedures, and evaluation of the method. Contrib Mineral Petrol 168:1033
814 doi:10.1007/s00410-014-1033-3

815 Gualda GAR, Ghiorso MS (2015) MELTS_Excel: A Microsoft Excel-based MELTS interface for research
816 and teaching of magma properties and evolution. Geochemistry, Geophysics, Geosystems : G3
817 16(1):315-324 doi:10.1002/2014GC005545

818 Gualda GAR, Ghiorso MS, Hurst AA, Allen MC, Bradshaw RW (2022) A complex patchwork of magma
819 bodies that fed the Bishop Tuff supereruption (Long Valley 1 caldera, CA, USA): Evidence from matrix
820 glass major and trace-element compositions. Frontiers in Earth Science
821 doi:10.3389/feart.2022.798387

822 Gualda GAR, Gravley DM, Connor M, Hollmann B, Pamukçu AS, Bégué F, . . . Deering CD (2018) Climbing
823 the crustal ladder: Magma storage-depth evolution during a volcanic flare-up. Science Advances
824 4(10):eaap7567 doi:10.1126/sciadv.aap7567

825 Gualda GAR, Gravley DM, Deering CD, Ghiorso MS (2019b) Magma extraction pressures and the
826 architecture of volcanic plumbing systems. Earth Planet Sci Lett 522:118-124
827 doi:10.1016/j.epsl.2019.06.020

828 Hammarstrom JM, Zen Ea (1986) Aluminum in hornblende; an empirical igneous geobarometer. Am
829 Mineral 71(11-12):1297-1313

830 Harmon LJ, Cowlyn J, Gualda GAR, Ghiorso MS (2018) Phase-equilibrium geobarometers for silicic rocks
831 based on rhyolite-MELTS. Part 4: Plagioclase, orthopyroxene, clinopyroxene, glass geobarometer, and
832 application to Mt. Ruapehu, New Zealand. Contrib Mineral Petrol 173(1):1-20 doi:10.1007/s00410-
833 017-1428-z

834 Harmon LJ, Gualda GA, Gravley DM, Smithies SL, Deering CD (2024a) The Whakamaru magmatic
835 system (Taupō Volcanic Zone, New Zealand), part 1: Evidence from tephra deposits for the eruption of
836 multiple magma types through time. J Volcanol Geotherm Res 445:107966

837 Harmon LJ, Gualda GA, Wallrich BM, Miller CF (2025) Shallow storage conditions at Krafla IDDP-1
838 revealed by rhyolite-MELTS geobarometry, and implications for global shallow magmatism. Earth
839 Planet Sci Lett 663:119421

840 Harmon LJ, Smithies SL, Gualda GA, Gravley DM (2024b) The Whakamaru Magmatic System (Taupō
841 Volcanic Zone, New Zealand), Part 2: Evidence from ignimbrite deposits for the pre-eruptive
842 distribution of melt-dominated magma and magma mushes. J Volcanol Geotherm Res:108013

843 Herzberg C (2004) Partial crystallization of mid-ocean ridge basalts in the crust and mantle. J Petrol
844 45(12):2389-2405

845 Holland T, Blundy J (1994) Non-ideal interactions in calcic amphiboles and their bearing on amphibole-
846 plagioclase thermometry. Contrib Mineral Petrol 116:433-447

847 Jay J, Costa F, Pritchard M, Lara L, Singer B, Herrin J (2014) Locating magma reservoirs using InSAR and
848 petrology before and during the 2011–2012 Cordón Caulle silicic eruption. Earth Planet Sci Lett
849 395:254-266

850 Johannes W, Holtz F (1996) Petrogenesis and experimental petrology of granitic rocks. Springer, Berlin

851 Jorgenson C, Higgins O, Petrelli M, Bégué F, Caricchi L (2022) A machine learning-based approach to
852 clinopyroxene thermobarometry: Model optimization and distribution for use in Earth sciences. J
853 Geophys Res Solid Earth 127(4):e2021JB022904

854 Karhunen RA (1993) The Pokai and Chimp ignimbrites of NW Taupo Volcanic Zone. PhD. University of
855 Canterbury

856 Kilgour G, Blundy J, Cashman K, Mader HM (2013) Small volume andesite magmas and melt–mush
857 interactions at Ruapehu, New Zealand: evidence from melt inclusions. Contrib Mineral Petrol
858 166(2):371-392

859 Lara L, Moreno H, Naranjo J, Matthews S, De Arce CP (2006) Magmatic evolution of the Puyehue–
860 Cordón Caulle Volcanic Complex (40 S), Southern Andean Volcanic Zone: from shield to unusual
861 rhyolitic fissure volcanism. J Volcanol Geotherm Res 157(4):343-366

862 Leonard GS (2003) The evolution of Maroa Volcanic Centre, Taupo Volcanic Zone, New Zealand. PhD.
863 University of Canterbury

864 Liu Y, Zhang Y, Behrens H (2005) Solubility of H2O in rhyolitic melts at low pressures and a new empirical
865 model for mixed H2O–CO2 solubility in rhyolitic melts. J Volcanol Geotherm Res 143(1-3):219-235

Magee C, Stevenson CT, Ebmeier SK, Keir D, Hammond JO, Gottsmann JH, . . . Petronis MS (2018) Magma plumbing systems: a geophysical perspective. J Petrol 59(6):1217-1251

Milner DM, Cole JW, Wood CP (2003) Mamaku Ignimbrite: a caldera-forming ignimbrite erupted from a compositionally zoned magma chamber in Taupo Volcanic Zone, New Zealand. J Volcanol Geotherm Res 122(3):243-264 doi:10.1016/S0377-0273(02)00504-8

Mingo MA (2019) Evaluation of Pre-eruptive Conditions for Cordon Caulle Rhyo-Dacitic Historic Eruptions. Florida International University

Molina JF, Cambeses A, Moreno JA, Morales I, Montero P, Bea F (2021) A reassessment of the amphibole-plagioclase NaSi-CaAl exchange thermometer with applications to igneous and high-grade metamorphic rocks. American Mineralogist 106(5):782-800

Mutch E, Blundy J, Tattitch B, Cooper F, Brooker R (2016) An experimental study of amphibole stability in low-pressure granitic magmas and a revised Al-in-hornblende geobarometer. Contrib Mineral Petrol 171:1-27

Newman S, Lowenstern JB (2002) VolatileCalc: a silicate melt–H2O–CO2 solution model written in Visual Basic for Excel. Computers & Geosciences 28(5):597-604 doi:10.1016/S0098-3004(01)00081-4

Pamukçu AS, Gualda GAR, Ghiorso MS, Miller CF, McCracken RG (2015) Phase-equilibrium geobarometers for silicic rocks based on rhyolite-MELTS—Part 3: Application to the Peach Spring Tuff (Arizona–California–Nevada, USA). Contrib Mineral Petrol 169(3):549 doi:10.1007/s00410-015-1122-y

Pamukçu AS, Gualda GAR, Gravley DM (2021) Rhyolite-MELTS and the storage and extraction of large-volume crystal-poor rhyolitic melts at the Taupō Volcanic Center: a reply to Wilson et al. (2021). Contrib Mineral Petrol 176(10):82 doi:10.1007/s00410-021-01840-2

Pamukçu AS, Wright KA, Gualda GAR, Gravley D (2020) Magma residence and eruption at the Taupo Volcanic Center (Taupo Volcanic Zone, New Zealand): insights from rhyolite-MELTS geobarometry, diffusion chronometry, and crystal textures. Contrib Mineral Petrol 175(5) doi:10.1007/s00410-020-01684-2

Papale P, Moretti R, Barbato D (2006) The compositional dependence of the saturation surface of H2O+ CO2 fluids in silicate melts. Chemical Geology 229(1-3):78-95

Pearce NJ, Westgate JA, Gualda GA, Gatti E, Muhammad RF (2020) Tephra glass chemistry provides storage and discharge details of five magma reservoirs which fed the 75 ka Youngest Toba Tuff eruption, northern Sumatra. Journal of Quaternary Science 35(1-2):256-271

Pistolesi M, Cioni R, Bonadonna C, Elissondo M, Baumann V, Bertagnini A, . . . Francalanci L (2015) Complex dynamics of small-moderate volcanic events: the example of the 2011 rhyolitic Cordón Caulle eruption, Chile. Bulletin of Volcanology 77:1-24

Pitcher BW, Gualda GA, Hasegawa T (2021) Repetitive duality of rhyolite compositions, timescales, and storage and extraction conditions for pleistocene caldera-forming eruptions, Hokkaido, Japan. J Petrol 62(2):egaa106

Pritchard M, De Silva S, Michelfelder G, Zandt G, McNutt SR, Gottsmann J, . . . Finnegan N (2018) Synthesis: PLUTONS: Investigating the relationship between pluton growth and volcanism in the Central Andes. Geosphere 14(3):954-982

905 Putirka KD (2008) Thermometers and barometers for volcanic systems. Reviews in Mineralogy and
906 Geochemistry 69(1):61-120

907 Ridolfi F, Renzulli A, Puerini M (2010) Stability and chemical equilibrium of amphibole in calc-alkaline
908 magmas; an overview, new thermobarometric formulations and application to subduction-related
909 volcanoes. Contrib Mineral Petrol 160(1):45-66 doi:10.1007/s00410-009-0465-7

910 Ruefer AC, Kelly LJ, Gualda GA, Carrillo EL, Hickernell S, Ward S, . . . Ruprecht P (2025) In one step:
911 Insights into shallow differentiation from basalt to rhyolite at Cordón Caulle from rhyolite-MELTS
912 simulations. J Volcanol Geotherm Res 462:108305

913 Schipper CI, Castro JM, Kennedy BM, Christenson BW, Aiuppa A, Alloway B, . . . Tuffen H (2019) Halogen
914 (Cl, F) release during explosive, effusive, and intrusive phases of the 2011 rhyolitic eruption at Cordón
915 Caulle volcano (Chile). Volcanica 2(1):73-90

916 Seropian G, Schipper CI, Harmon LJ, Smithies SL, Kennedy BM, Castro JM, . . . Forte P (2021) A century
917 of ongoing silicic volcanism at Cordon Caulle, Chile; new constraints on the magmatic system involved
918 in the 1921-1922, 1960 and 2011-2012 eruptions. J Volcanol Geotherm Res 420:107406
919 doi:10.1016/j.jvolgeores.2021.107406

920 Singer BS, Jicha BR, Harper MA, Naranjo JA, Lara LE, Moreno-Roa H (2008) Eruptive history,
921 geochronology, and magmatic evolution of the Puyehue-Cordón Caulle volcanic complex, Chile. Geol
922 Soc Am Bull 120(5-6):599-618

923 Smithies SL, Gravley DM, Gualda GA (2024) Connecting the Dots: the Lava Domes' Perspective of
924 Magmatism Related to an Ignimbrite Flare-Up. J Petrol 65(01):egad090

925 Smithies SL, Harmon LJ, Allen SM, Gravley DM, Gualda GAR (2023) Following magma: The pathway of
926 silicic magmas from extraction to storage during an ignimbrite flare-up, Taupō Volcanic Zone, New
927 Zealand. Earth Planet Sci Lett 607:118053 doi:10.1016/j.epsl.2023.118053

928 Tomiya A, Miyagi I, Saito G, Geshi N (2013) Short time scales of magma-mixing processes prior to the
929 2011 eruption of Shinmoedake volcano, Kirishima volcanic group, Japan. Bulletin of Volcanology 75:1-
930 19

931 Ubide T, Wieser PE, Bachmann O, Gualda GAR, Neave DA, Samaniego P, Kent A (in press) Petrological
932 characterisation of magma storage. In: Bonadonna C, Caricchi L, Clarke A, Cole P, Lindsay JM,
933 Lowenstern JB, Robertson R, Martinez-Villegas MM (eds) The Encyclopedia of Volcanoes, vol 1.
934 https://doi.org/10.31223/X5NX44

935 Van Orman JA, Crispin KL (2010) Diffusion in oxides. Reviews in Mineralogy and Geochemistry
936 72(1):757-825

937 Voigt M, Coogan LA, von der Handt A (2017) Experimental investigation of the stability of clinopyroxene
938 in mid-ocean ridge basalts: the role of Cr and Ca/Al. Lithos 274:240-253

939 Wallace PJ, Anderson AT, Davis AM (1995) Quantification of pre-eruptive exsolved gas contents in silicic
940 magmas. Nature 377(6550):612-616

941 Weber G, Blundy J (2024) A machine learning-based thermobarometer for magmatic liquids. J
942 Petrol:egae020

943 Wendt A, Tassara A, Báez JC, Basualto D, Lara LE, García F (2017) Possible structural control on the
944 2011 eruption of Puyehue-Cordón Caulle Volcanic Complex (southern Chile) determined by InSAR, GPS
945 and seismicity. Geophysical Journal International 208(1):134-147

946 Wieser PE, Gleeson MLM, Matthews S, DeVitre C, Gazel E (2025) Determining the pressure-
947 temperature-composition (P-T-X) conditions of magma storage. In: Anbar A, Weis D (eds) Treatise on
948 Geochemistry (Third edition), vol 2. Elsevier, pp 83-151

949 Wieser PE, Kent AJ, Till CB, Abers GA (2023a) Geophysical and geochemical constraints on magma
950 storage depths along the Cascade arc: Knowns and unknowns. Geochemistry, Geophysics, Geosystems
951 24(11):e2023GC011025

952 Wieser PE, Kent AJ, Till CB, Donovan J, Neave DA, Blatter DL, Krawczynski MJ (2023b) Barometers
953 behaving badly I: Assessing the influence of analytical and experimental uncertainty on clinopyroxene
954 thermobarometry calculations at crustal conditions. J Petrol 64(2):egac126

955 Wilke S, Holtz F, Neave DA, Almeev R (2017) The effect of anorthite content and water on quartz-
956 feldspar cotectic compositions in the rhyolitic system and implications for geobarometry. J Petrol
957 58(4):789-818 doi:10.1093/petrology/egx034

958 Winslow H, Ruprecht P, Gonnermann HM, Phelps PR, Muñoz-Saez C, Delgado F, . . . Amigo A (2022)
959 Insights for crystal mush storage utilizing mafic enclaves from the 2011-12 Cordón Caulle eruption.
960 Scientific Reports 12(1):9734-9734 doi:10.1038/s41598-022-13305-y

961 Yang H-J, Kinzler RJ, Grove TL (1996) Experiments and models of anhydrous, basaltic olivine-
962 plagioclase-augite saturated melts from 0.001 to 10 kbar. Contrib Mineral Petrol 124(1):1-18

963

964